pre-existing immunity against the parent Ads (Table 2 and Figure 4). The exchange of other genes, including hexon and penton, may further reduce the inhibition of pre-existing anti-Ad5 immunity. (2) We also explored the immune responses by using the same vector for prime/boost. When the mice were immunized i.m. with 10^{10} vp of Ad5/35-HIV 1–3 times at 4-week intervals, the HIV-specific cell-mediated immune responses were detected by the tetramer assay. An increased response was observed after the second immunization but not after the third immunization (data not shown). High anti-Ad5/35 neutralizing Ab after second immunization may block the Ad5/35-HIV infection (Figure 4). These results are in agreement with the data from our study on monkeys (Figure 3b and c) and with that from studies by other groups,[33,43] and other virus such as MVA vector may be applicable for further boost if high immune responses are required. The DNA-HIV vaccine prime/Ad5/35-HIV vector boost regimen greatly increased HIV-specific cell-mediated immune responses (Table 1 and Figure 3b and c), but not the humoral immune response (Figure 2c). This suggests that DNA vaccination enhances adenoviral recombinant-induced cell-mediated immunity rather than humoral immunity, as described by other groups.[4,38] Furthermore, DNA vaccine priming can reduce the humoral response to the adenoviral antigens and can counterbalance the impaired B-cell response to the antigen expressed by the adenoviral recombinant in mice that are preimmune to Ad.[46] This DNA prime/Ad5/35 boost regimen might be highly suitable for use in humans with previous exposure to the Ad5 virus. (3) To examine the immunogenicity and protective immunity of the Ad5/35 vector, we used HIV-1 IIIB in this study, because the strain has been well studied and we can compare our data from the new vector with that from other studies. For the clinical trail, we have constructed DNA vaccine and Ad5/5 vector expressing ENV and GAG of a Clade C HIV-1 isolate and similar results with HIV-1 IIIB strain were obtained in a mouse model (manuscript in preparation).

Considered together, using Ad5/35 vector, we developed an HIV vaccine with a higher immunogenicity and low pathogenicity. The Ad5/35-HIV vaccine induced strong HIV-specific immune responses in both BALB/c mice and rhesus monkeys. Priming with a DNA-HIV vaccine followed by Ad5/35-HIV boosting yielded protection against viral infection in mice. The Ad5/35 vector may be a promising vaccine for human clinical trial.

Materials and methods

Recombinant vectors

E1,E3-deletion, replication-defective recombinant viruses were constructed with an Ad generation kit (Avior Therapeutics Inc., Seattle, WA, USA).[21] Briefly, a 5.2k bp *Sal*I/*Pst*I fragment containing CAG promoter-HIV_{IIIB} rev/env gp160-polyA was isolated from pCAGrev/env.[28] A shuttle plasmid (pLHSP) containing Ad5 positions 22–342, Ad5 3523–5790, *Escherichia coli ori*, and ampicillin-resistant gene was obtained from Avior Therapeutics Inc. (Seattle, WA, USA). The 5.2k bp blunted fragment was subcloned into blunted *Eco*RI site of pLHSP plasmid vector to generate pLHSP-HIV shuttle plasmid. The pLHSP-HIV shuttle plasmid was linearized with *Pac*I and transfected with E1,E3-deletion, chimeric Ad5 or 5/35 genome to human embryonic kidney (HEK293) cells using calcium precipitation method to generate recombinant virus, Ad5-HIV and Ad5/35-HIV, respectively. The recombinant virus (Ad5/35-HIV, Ad5-HIV) was propagated in HEK293 cells and purified by two repetitions of the CsCl methods described elsewhere.[47] The total concentration of virions in each preparation was calculated from the optical density at 260 nm (OD_{260}), using the formula 1 $OD_{260} = 1 \times 10^{12}$ vp/ml. The HIV_{BH8} gp160-expressing replication-competent vaccinia virus (WR strain, vPE16; HIV_{BH8} gp160 has 97.32% amino-acid homology with HIV_{IIIB} gp160) was obtained from the AIDS Research and Reagent Program, National Institutes of Health, Rockville, MD, USA (Cat. No. 362). The vPE16 vectors were propagated in CV1 cells. The Ad5-Luc and Ad5/35-Luc vectors expressing luciferase coding gene were described previously.[26] The DNA-HIV vaccine (pCAGrev/env) containing HIV_{IIIB} *rev* and *env* genes has been previously reported.[28]

Biodistribution of Ad5 and Ad5/35 vectors in vivo

The experiment was performed as previously described.[48,49] In brief, the Ad5-Luc or Ad5/35-Luc vectors (10^{11} vp/mouse) were injected i.m. into BALB/c mice. On days 3 and 10, the mice were anesthetized with a 2% isofluorane/air mixture, and a single dose of 150 mg/kg luciferin in normal saline was administered intraperitoneally. The CCD images were obtained using a cooled *in vivo* imaging system (IVIS) CCD camera (Xenogen, Alameda, CA, USA) and analyzed. To study the viral biodistribution in primates, two rhesus monkeys (2 years old, male) were administered i.m. 10^{11} vp of Ad5-Luc or Ad5/35-Luc. At 3 days after administration, the luciferase activity was detected in the monkey organs (brain, liver, kidney, spleen, heart, and lung) using the Luciferase Assay Systems (Promega, Madison, WI, USA). Serum GOT and serum GPT were measured in mouse or monkey sera at the Kitayama-Rabesu Institute (Ina, Nagano, Japan). The concentration of serum IFN-γ and IL-6 was measured using the IFN-γ and IL-6 ELISA kits (Biosource, Camarillo, CA, USA), respectively, according to the manufacturer's protocol.

Animal immunization

Female BALB/c mice (8-week-old; $H\text{-}2D^d$) were purchased from Japan SLC Inc., Shizuoka, Shizuoka-ken, Japan. The mice were immunized with an i.m. injection of 100 μg of pCAGrev/env or pCAGempty plasmid DNA in phosphate-buffered saline (PBS) at 0, 1, and 2 weeks and were boosted with 10^{10} vp of Ad5/35-HIV or Ad5/35-Luc vector at week 3. For the time-course study, the mice were administered a single i.m. injection of 10^{10} vp of Ad5/35-HIV vector per mouse. To study the effect of pre-existing antiviral immunity on vaccination, the mice were injected i.m. with 10^{10} or 10^{11} vp of Ad5-Luc vector and then immunized 8 weeks later with 10^{10} vp of Ad5-HIV vector or Ad5/35-HIV vector. For rhesus monkey immunization, 10^{11} vp of Ad5/35-HIV vector was injected i.m. into two rhesus monkeys (2 years old, male) at weeks 0 and 8.

Intracellular cytokine staining assay

IFN-γ-secreting $CD8^+$ T cells were detected by the protocol recommended by the manufacturer (Cytofix/CytoPerm Plus kit, PharMingen, San Diego, CA, USA). In brief, lymphocytes were isolated from the mouse spleen. A single cell suspension was incubated with 10 μg/ml of the HIV V3 peptide (NNTRKRIQRGP GRAFVTIGKIGN) for 24 h at 37°C. At 2 h before the end of incubation, 1 μg/ml of GolgiPlug was added. The cells were washed with staining buffer (3% fetal calf serum (FCS), 0.1% sodium azide (NaN_3) in PBS), blocked with 4% normal mouse sera, and stained with phycoerythrin (PE)-conjugated anti-mouse CD8 Ab (Ly-2, PharMingen). The cells were then suspended in 250 μl of Cytofix/Cytoperm solution at 4°C for 20 min, washed with Perm/Wash solution, and stained with anti-mouse IFN-γ Ab conjugated with fluorescein isothiocyanate (FITC) (PharMingen) at 4°C for 30 min, followed by flow cytometric analysis.

Tetramer assay

The tetramer assay used a PE-conjugated $H\text{-}2D^d/p18$ tetramer (RGPGRAFVTI), as previously described.[28] In brief, splenocytes were isolated from mice and incubated for 30 min at 4°C with 4% normal mouse serum in PBS. Cells were stained with FITC-conjugated anti-mouse CD8 Ab (Ly-2, PharMingen) for 30 min at 4°C. After washing twice with the staining buffer (3% FCS, 0.1% NaN_3 in PBS), the cells were incubated with the tetramer reagent for 15 min at 37°C, followed by flow cytometric analysis (Becton Dickinson).

Recombinant vaccinia virus used for the challenge study

Using vPE16 vaccinia virus, the virus challenge experiment was performed as described previously.[28] Vaccinated female mice were intraperitoneally challenged with 10^8 PFU of vaccinia virus vPE16 at 2 or 7 weeks after the final immunization. At 6 days after challenge, the mice were killed, their ovaries were sonicated, and the vPE16 titer was determined by serial 10-fold dilution on a plate of CV1 cells. Infected cells were detected by staining with crystal violet and plaques were counted at each dilution.

Detection of HIV-1-specific Ab

The HIV-1-specific Ab was detected by the Western blotting method and the enzyme-linked immunosorbent assay (ELISA). By Western blotting method, the HIV envelope glycoprotein gp160-coated membrane from the New Lav Blot 1 kit (Bio-Rad, Marnes-la-Coquette, France) was incubated with a 100-fold dilution of mouse serum followed by an affinity-purified horseradish peroxidase (HRP)-labeled anti-mouse immunoglobulin (ICN Pharmaceuticals Inc., OH, USA). HIV gp160 protein was detected using the ECL Plus Western Blotting Detection System (Amersham Pharmacia Biotech).

ELISA was performed as described elsewhere.[10] To summarize, 96-well microtiter plates were coated with 10 μg/ml of HIV_{IIIB} gp120 protein (donated by AIDS Research and Reference Reagent Program, National Institutes of Health) and incubated overnight at 4°C. The wells were blocked with PBS containing 1% bovine serum albumin (BSA) for 2 h at room temperature. They were then treated with 100 μl of serially diluted antisera and incubated for an additional 2 h at 37°C. The bound immunoglobulin was quantified using an affinity-purified HRP-labeled anti-mouse Ab or anti-monkey Ab (both from Sigma). The mean Ab titer was expressed as the reciprocal of the serial serum dilution that exceeded the assay background by 2 s.d.

The HIV-specific neutralizing titer of immune mice or monkeys was also measured. The serially diluted antisera were incubated with 200–300 blue spot-forming units (BFU) of $HIV\text{-}1_{LAI}$ at 37°C for 1 h. The mixture was incubated with confluent MAGIC5 cells (from Dr Tatsumi, National Institute of Infectious Diseases, Tokyo, Japan),[50,51] Dulbecco's modified Eagle's medium (DMEM) with 10% FCS and 0.2 mg/ml of G418 in a 96-well plate at 37°C for 2 days. The cells were fixed with fixing solution (1% formaldehyde, 0.2% glutaraldehyde in PBS) for 5 min and stained with staining solution (4 mM potassium ferrocyanide, 4 mM potassium ferricyanide, 2 mM magnesium chloride, 0.4 mg/ml X-gal in PBS) at 37°C for 18–24 h. The staining was stopped by removing the staining solution and the cells were washed twice with PBS. The blue spot in each well was counted after the staining, and the neutralizing titer was calculated as $(1-(\%\ \text{infection}/\%\ \text{infection of control wells})) \times 100$. The 50% neutralization dose (ND_{50}) is defined as the concentration of the Ab that reduced the number of infected cells by 50%. The detecting limitation of the assay was 100 ND_{50}/ml.

ELISPOT assay

The frequency of HIV-specific IFN-γ-secreting cells in monkeys was determined using an ELISPOT assay kit (U-Cytech, Utrech, The Netherlands) according to the manufacturer's manual. In brief, 2×10^5 monkey PBMCs were stimulated in triplicate wells with 1 μg/ml of the HIV_{IIIB} gp120 protein for 16 h at 37°C. Nonstimulated cells were used to assess the background. The cells were transferred to an anti-IFN-γ Ab-coated 96-well plate and incubated for 5 h at 37°C. The cells were removed and 200 μl/well of ice-cold deionized water was added to lyse the remaining PBMCs. Subsequently, the plate was washed with PBS containing 0.05% Tween 20 (PBS-T) and incubated with biotinylated anti-IFN-γ Ab for 1 h at 37°C. After 10 washings with PBS-T, 50 μl of gold-labeled anti-biotin Ab was added and incubated for 1 h at 37°C. The plate was washed 10 times with PBS-T, and 30 ml of activator solutions was added. The plate was incubated in the dark for 30 min at room temperature to develop spot formations. After 30 min incubation, the plate was washed with deionized water and air-dried; spots were counted by a computer-assisted video image analysis. The results were expressed as spot-forming cells (SFC) per million cells.

Ad-specific neutralizing assay

Ad5-Luc or Ad5/35-Luc vector (10^7 vp) was incubated with an equal volume of serially diluted normal human sera (anti-Ad5 neutralizing titer <1:4), human antisera (anti-Ad5 neutralizing titer = 1:64), or monkey sera (at weeks 0, 2, 8, and 12 after immunization with Ad5/35-HIV vector) at 37°C for 2 h. The mixture was incubated with confluent Vero cells in a 96-well plate at 37°C for an additional 48 h. The luciferase activity was detected by Luciferase Assay Systems (Promega, Madison, WI, USA).

The neutralizing titer was calculated with limited serum dilution when the luciferase activity in the Ad-infected cells was equal with the background.

Data analysis

All values were expressed as means ± standard error (s.e.). Statistical analysis of the experimental data and controls was conducted with one-way factorial analysis of variance. Significance was defined at $P<0.05$ in the statistical analysis.

Acknowledgements

We are grateful to M Kawano, T Takeishi, and T Matsuda for their technical assistance and A De La Fuente for her secretarial assistance. This work was partially supported by a Grant-in-Aid from the Ministry of Education, Science, Sports, and Culture of Japan, and the grant for 2005 Strategic Research Project (No. K17018) of Yokohama City University, Japan.

References

1 Bukawa H *et al.* Neutralization of HIV-1 by secretory IgA induced by oral immunization with a new macromolecular multicomponent peptide vaccine candidate. *Nat Med* 1995; **1**: 681–685.
2 Barouch DH *et al.* Control of viremia and prevention of clinical AIDS in rhesus monkeys by cytokine-augmented DNA vaccination. *Science* 2000; **290**: 486–492.
3 Robinson HL *et al.* Neutralizing antibody-independent containment of immunodeficiency virus challenges by DNA priming and recombinant pox virus booster immunizations. *Nat Med* 1999; **5**: 526–534.
4 Shiver JW *et al.* Replication-incompetent adenoviral vaccine vector elicits effective anti-immunodeficiency-virus immunity. *Nature* 2002; **415**: 331–335.
5 Patterson LJ *et al.* Protection against mucosal simian immunodeficiency virus SIV(mac251) challenge by using replicating adenovirus-SIV multigene vaccine priming and subunit boosting. *J Virol* 2004; **78**: 2212–2221.
6 Schnell MJ *et al.* Recombinant rabies virus as potential live-viral vaccines for HIV-1. *Proc Natl Acad Sci USA* 2000; **97**: 3544–3549.
7 Mandl CW *et al. In vitro*-synthesized infectious RNA as an attenuated live vaccine in a flavivirus model. *Nat Med* 1998; **4**: 1438–1440.
8 Matano T *et al.* Cytotoxic T lymphocyte-based control of simian immunodeficiency virus replication in a preclinical AIDS vaccine trial. *J Exp Med* 2004; **199**: 1709–1718.
9 Caley IJ *et al.* Venezuelan equine encephalitis virus vectors expressing HIV-1 proteins: vector design strategies for improved vaccine efficacy. *Vaccine* 1999; **17**: 3124–3135.
10 Xin KQ *et al.* Oral administration of recombinant adeno-associated virus elicits human immunodeficiency virus-specific immune responses. *Hum Gene Ther* 2002; **13**: 1571–1581.
11 Xin KQ *et al.* A novel recombinant adeno-associated virus vaccine induces a long-term humoral immune response to human immunodeficiency virus. *Hum Gene Ther* 2001; **12**: 1047–1061.
12 Aldovini A, Young RA. Humoral and cell-mediated immune responses to live recombinant BCG-HIV vaccines. *Nature* 1991; **351**: 479–482.
13 Someya K *et al.* Vaccination of rhesus macaques with recombinant *Mycobacterium bovis* bacillus Calmette–Guerin Env V3 elicits neutralizing antibody-mediated protection against simian-human immunodeficiency virus with a homologous but not a heterologous V3 motif. *J Virol* 2005; **79**: 1452–1462.
14 Xin KQ *et al.* Immunogenicity and protective efficacy of orally administered recombinant *Lactococcus lactis* expressing surface-bound HIV Env. *Blood* 2003; **102**: 223–228.
15 Sullivan NJ *et al.* Development of a preventive vaccine for Ebola virus infection in primates. *Nature* 2000; **408**: 605–609.
16 Amara RR *et al.* Different patterns of immune responses but similar control of a simian-human immunodeficiency virus 89.6P mucosal challenge by modified vaccinia virus Ankara (MVA) and DNA/MVA vaccines. *J Virol* 2002; **76**: 7625–7631.
17 Vogels R *et al.* Replication-deficient human adenovirus type 35 vectors for gene transfer and vaccination: efficient human cell infection and bypass of preexisting adenovirus immunity. *J Virol* 2003; **77**: 8263–8271.
18 Havenga MJ *et al.* Exploiting the natural diversity in adenovirus tropism for therapy and prevention of disease. *J Virol* 2002; **76**: 4612–4620.
19 Roelvink PW *et al.* The coxsackievirus-adenovirus receptor protein can function as a cellular attachment protein for adenovirus serotypes from subgroups A, C, D, E, and F. *J Virol* 1998; **72**: 7909–7915.
20 Sakurai F, Mizuguchi H, Yamaguchi T, Hayakawa T. Characterization of *in vitro* and *in vivo* gene transfer properties of adenovirus serotype 35 vector. *Mol Ther* 2003; **8**: 813–821.
21 Shayakhmetov DM, Papayannopoulou T, Stamatoyannopoulos G, Lieber A. Efficient gene transfer into human CD34(+) cells by a retargeted adenovirus vector. *J Virol* 2000; **74**: 2567–2583.
22 Adams JY *et al.* Visualization of advanced human prostate cancer lesions in living mice by a targeted gene transfer vector and optical imaging. *Nat Med* 2002; **8**: 891–897.
23 Thomas CE, Ehrhardt A, Kay MA. Progress and problems with the use of viral vectors for gene therapy. *Nat Rev Genet* 2003; **4**: 346–358.
24 Gao W, Robbins PD, Gambotto A. Human adenovirus type 35: nucleotide sequence and vector development. *Gene Therapy* 2003; **10**: 1941–1949.
25 Gaggar A, Shayakhmetov DM, Lieber A. CD46 is a cellular receptor for group B adenoviruses. *Nat Med* 2003; **9**: 1408–1412.
26 Mizuguchi H, Hayakawa T. Adenovirus vectors containing chimeric type 5 and type 35 fiber proteins exhibit altered and expanded tropism and increase the size limit of foreign genes. *Gene* 2002; **285**: 69–77.
27 Seshidhar Reddy P *et al.* Development of adenovirus serotype 35 as a gene transfer vector. *Virology* 2003; **311**: 384–393.
28 Jounai N *et al.* Contribution of the *rev* gene to the immunogenicity of DNA vaccines targeting the envelope glycoprotein of HIV. *J Gene Med* 2003; **5**: 609–617.
29 Maino VC, Picker LJ. Identification of functional subsets by flow cytometry: intracellular detection of cytokine expression. *Cytometry* 1998; **34**: 207–215.
30 Letvin NL *et al.* Heterologous envelope immunogens contribute to AIDS vaccine protection in rhesus monkeys. *J Virol* 2004; **78**: 7490–7497.
31 Barouch DH *et al.* Reduction of simian-human immunodeficiency virus 89.6P viremia in rhesus monkeys by recombinant modified vaccinia virus Ankara vaccination. *J Virol* 2001; **75**: 5151–5158.
32 Altman JD *et al.* Phenotypic analysis of antigen-specific T lymphocytes. *Science* 1996; **274**: 94–96.
33 Sullivan NJ *et al.* Accelerated vaccination for Ebola virus haemorrhagic fever in non-human primates. *Nature* 2003; **424**: 681–684.
34 Wadell G. Molecular epidemiology of human adenoviruses. *Curr Top Microbiol Immunol* 1984; **110**: 191–220.
35 De Jong JC *et al.* Adenoviruses from human immunodeficiency virus-infected individuals, including two strains that represent new candidate serotypes Ad50 and Ad51 of species B1 and D, respectively. *J Clin Microbiol* 1999; **37**: 3940–3945.

36 Kostense S *et al.* Adenovirus types 5 and 35 seroprevalence in AIDS risk groups supports type 35 as a vaccine vector. *Aids* 2004; **18**: 1213–1216.
37 Barouch DH *et al.* Immunogenicity of recombinant adenovirus serotype 35 vaccine in the presence of pre-existing anti-Ad5 immunity. *J Immunol* 2004; **172**: 6290–6297.
38 Casimiro DR *et al.* Comparative immunogenicity in rhesus monkeys of DNA plasmid, recombinant vaccinia virus, and replication-defective adenovirus vectors expressing a human immunodeficiency virus type 1 *gag* gene. *J Virol* 2003; **77**: 6305–6313.
39 Morral N *et al.* Administration of helper-dependent adenoviral vectors and sequential delivery of different vector serotype for long-term liver-directed gene transfer in baboons. *Proc Natl Acad Sci USA* 1999; **96**: 12816–12821.
40 Hofmann C *et al.* Ovine adenovirus vectors overcome preexisting humoral immunity against human adenoviruses *in vivo*. *J Virol* 1999; **73**: 6930–6936.
41 Farina SF *et al.* Replication-defective vector based on a chimpanzee adenovirus. *J Virol* 2001; **75**: 11603–11613.
42 Moffatt S, Hays J, HogenEsch H, Mittal SK. Circumvention of vector-specific neutralizing antibody response by alternating use of human and non-human adenoviruses: implications in gene therapy. *Virology* 2000; **272**: 159–167.
43 Pinto AR *et al.* Induction of CD8+ T cells to an HIV-1 antigen through a prime boost regimen with heterologous E1-deleted adenoviral vaccine carriers. *J Immunol* 2003; **171**: 6774–6779.
44 Fitzgerald JC *et al.* A simian replication-defective adenoviral recombinant vaccine to HIV-1 *gag*. *J Immunol* 2003; **170**: 1416–1422.
45 Lemiale F *et al.* Enhanced mucosal immunoglobulin A response of intranasal adenoviral vector human immunodeficiency virus vaccine and localization in the central nervous system. *J Virol* 2003; **77**: 10078–10087.
46 Xiang ZQ, Pasquini S, Ertl HC. Induction of genital immunity by DNA priming and intranasal booster immunization with a replication-defective adenoviral recombinant. *J Immunol* 1999; **162**: 6716–6723.
47 Lieber A, He CY, Kirillova I, Kay MA. Recombinant adenoviruses with large deletions generated by Cre-mediated excision exhibit different biological properties compared with first-generation vectors *in vitro* and *in vivo*. *J Virol* 1996; **70**: 8944–8960.
48 Bhaumik S, Gambhir SS. Optical imaging of *Renilla* luciferase reporter gene expression in living mice. *Proc Natl Acad Sci USA* 2002; **99**: 377–382.
49 Lipshutz GS *et al. In utero* delivery of adeno-associated viral vectors: intraperitoneal gene transfer produces long-term expression. *Mol Ther* 2001; **3**: 284–292.
50 Mochizuki N *et al.* An infectious DNA clone of HIV type 1 subtype C. *AIDS Res Hum Retroviruses* 1999; **15**: 1321–1324.
51 Mukai T *et al.* Construction and characterization of an infectious molecular clone derived from the CRF01_AE primary isolate of HIV type 1. *AIDS Res Hum Retroviruses* 2002; **18**: 585–589.

International Immunology, Vol. 17, No. 5, pp. 513–522
doi:10.1093/intimm/dxh231

Anti-CD3 induces bi-phasic apoptosis in murine intestinal epithelial cells: possible involvement of the Fas/Fas ligand system in different T cell compartments

Naoko Miura[1], Masahiro Yamamoto[1], Masato Fukutake[1], Nobuhiro Ohtake[1], Seiichi Iizuka[1], Atsushi Ishige[1], Hiroshi Sasaki[1], Kazunori Fukuda[2], Tatsuo Yamamoto[3] and **Satoshi Hayakawa[3]**

[1]Tsumura Research Institute, Tsumura & Co., 3586 Yoshiwara, Ami-machi, Inashiki-gun, Ibaraki 300-1192, Japan
[2]Department of Oriental Medicine, Gifu University School of Medicine, Gifu, Japan
[3]Department of Obstetrics and Gynaecology, Nihon University School of Medicine, Tokyo, Japan

Keywords: crypt, intestinal injury, intestinal intraepithelial lymphocytes, splenocytes, villus

Abstract

Recent studies have suggested that Fas-mediated apoptosis is involved in the pathogenesis of intestinal injury. In this study, we determined the role of Fas/Fas ligand (FasL) interactions in different T cell compartments using a murine model of small intestinal injury. An intraperitoneal injection of 145-2C11 (anti-CD3) antibody into C3H/HeN, BALB/c and MRL mice induced mucosal flattening and rapid, bi-phasic intestinal epithelial cell (IEC) apoptosis, which was detected by conventional light and electron microscopy and by terminal deoxynucleotidyl transferase-mediated dUTP nick-end labeling. In the first, early phase, villous apoptosis was observed up to 4 h after injection, and in the second, later phase, apoptotic crypt cells gradually accumulated for up to 24 h. The early and later phases of apoptosis were reduced in *lpr/lpr* and nude mice compared with those in control strains. In addition, the kinetics of Fas-mediated killer activity induced by the antibody injection were different between intestinal intraepithelial lymphocytes (IEL) and splenocytes (SPL) and seemed to correlate with the bi-phasic occurrence of the apoptosis. Finally, the transfer of intestinal IEL from euthymic to nude mice induced both phases of apoptosis, whereas SPL induced the second phase's crypt apoptosis only by the antibody injection. Together, these results suggest the involvement of Fas-mediated killer activity of thymus-derived T cells in different compartments. Namely, T cell populations in different compartments are differentially involved in the induction of IEC apoptosis and contribute to the complex pathogenesis of immune-mediated intestinal injury in which Fas/FasL interactions may play a critical role.

Introduction

A consensus is emerging that T cells play a central role in the development of intestinal inflammation. Activated T cells are involved in both regulatory and effector mechanisms in inflammatory responses. The effector mechanisms are important for defense against enterobacteria, but may also cause significant bystander tissue damage such as villous atrophy, which may be due to increased intestinal epithelial cell (IEC) apoptosis. Indeed, abnormal T cell activation has been reported in some enteropathies, such as Crohn's disease, ulcerative colitis and celiac disease (1–3).

Activated T cells mediate cytotoxicity through several mechanisms, of which, the Fas/Fas ligand (FasL) system plays an important role. Recent studies have demonstrated that the FasL molecule is expressed on either systemic and/or mucosal lymphocytes in enteropathies such as ulcerative colitis (4, 5) and celiac disease (6–10). In animal models of intestinal injury, several studies have shown that Fas/FasL-mediated cytotoxicity by mucosal lymphocytes may be partly responsible for the enteropathy (11–15). The type and function of the immune components involved in intestinal damage are,

Correspondence to: N. Miura; E-mail: miura_naoko@mail.tsumura.co.jp

Transmitting editor: H. Kikutani

Received 8 April 2003, *accepted* 3 February 2005

Advance Access publication 18 March 2005

however, still obscure, partly because many players including the immune components are involved in the intestinal immune system. The gut-associated lymphoid tissue comprises four compartments: intestinal epithelium, lamina propria, Peyer's patches and mesenteric lymph nodes (16). Gut tissue is an intersection of the mucosal and systemic immune systems, and interactions between different types of T cells may be critical for the integrity of the intestinal immune system. In the inflammatory state, the infiltration of peripheral leukocytes into the tissue makes the situation far more complicated.

The purpose of this study was to investigate the possible involvement of different T cell compartments in killing IEC *in vivo* using a model of small intestinal injury. T cell activation was evoked systemically by the intraperitoneal administration of anti-CD3 antibody. A direct administration was performed in order to avoid any possible interactions between the stimulator and intestinal contents (food, digestive enzymes and bacterial flora). Then we assessed the involvement of Fas using *in vivo* antibody injection to Fas-deficient mice and *ex vivo* measurements of Fas-mediated killer activity after antibody injection. Further, we determined whether thymus-derived T cells were involved in the observed intestinal injury using nude mice. Finally, we investigated the role of intraepithelial lymphocytes (IEL) and splenocytes (SPL) using cell transfer experiments.

Methods

Animals and mAbs

Male C3H/HeN, MRL-+/+, MRL-*lpr/lpr* (Japan SLC Inc., Shizuoka, Japan), BALB/c and BALB/c *nu/nu* (Japan Charles River Laboratory, Yokohama, Japan) mice bred and maintained under specific pathogen-free conditions were used at 9–10 weeks of age. This study conformed to our institution's guidelines for the care and use of laboratory animals in research. Hamster anti-murine CD3 mAb (145-2C11) and control hamster IgG1κ were obtained from BD Biosciences (San Jose, CA, USA). For flow cytometry, we used FITC-conjugated antibodies against CD3 (145-2C11), CD69 (H1.2F3), Fas (Jo2), control hamster IgG1κ, IgG1λ, IgG2λ, PE-conjugated FasL (MFL3) and control hamster IgG1κ (BD Biosciences).

Histology

Mice that received a single intraperitoneal injection of titrated concentrations of anti-CD3 antibody diluted in 100 μl of saline were sacrificed at different time points. The small intestines were removed, fixed and embedded in paraffin according to routine procedures. We quantified apoptotic cells by the method used in the previous studies of the intestinal injury model with minor modifications (17–20). In brief, we have counted damaged cells that have condensing or fragmenting nuclei, classical and definitive features of apoptosis, by light microscopic observation of hematoxylin and eosin (H&E)-stained histological sections. Apoptotic cells in 21 pairs of an adjacent villus and crypt (hereafter the pair will be expressed as a 'villus per crypt unit') were counted in seven random high fields (×400 magnification) per mice. Data represent the number of apoptotic cells in a villus or crypt per unit separately. This classical method of detecting apoptosis is incomplete in terms of the determination of absolute number of apoptosis because of the presence of fragmented cell debris and the very early stage-apoptotic cells in which the changes in nuclei have not occurred yet, however, it can assess the degree of apoptosis at least enough to demonstrate the time- and site-dependent changes of apoptotic changes in small intestines. The terminal deoxynucleotidyl transferase-mediated dUTP nick-end labeling (TUNEL) assay (*In situ* apoptosis detection kit, Intergen Company, NY, USA) was used for only qualitative detection of DNA fragmentation because the TUNEL assay, when used to quantify IEC apoptosis, has been reported to give conflicting results (21). For electron microscopy, samples of small intestine were fixed in 2% glutaraldehyde and processed using routine methods.

Fas-mediated cytotoxicity assay

We analyzed the Fas-mediated cytotoxicity of lymphocytes obtained from mice after anti-CD3 injection. IEL, SPL, mesenteric lymph node cells (MLNC) and Peyer's patch lymphocytes (PPL) were prepared by the method of Taguchi *et al.* (22). The Fas-positive human cell line, Jurkat, was obtained from the American Type Culture Collection (Rockville, MD, USA). Fas-mediated cytotoxicity was assessed according to the method of Lin *et al.* (23), with modifications. This assay is based on the fact that both murine and human FasL can kill Jurkat cells equally well and that the observed cytotoxicity is exclusively dependent on Fas (24). Briefly, [^{3}H]thymidine-labeled Jurkat cells (2×10^4 per well) were cultured with freshly isolated lymphocytes at different Effecter/Target (E/T) ratios in flat-bottomed 96-well plates, previously coated or not coated with 7.4 μg ml^{-1} of anti-CD3 antibody. After cultivation, the cells were lysed and harvested onto two-layered filters: a diethylaminoethyl (DEAE) glass filter to trap fragmented DNA and an unmodified glass filter to trap intact chromatin (25). The percentage of DNA fragmentation was calculated as follows:

$$\%\,\text{DNA fragmentation} = \{\text{c.p.m. DEAE filter}/(\text{c.p.m. glass filter} + \text{c.p.m. DEAE filter})\} \times 100.$$

The expression of cell surface markers was analyzed by flow cytometry (FACScan, BD Biosciences), and data were processed using the Macintosh CELLQuest program (BD Biosciences).

Adoptive transfer of immune cells

Experiment 1. Freshly isolated SPL (5×10^7) or IEL (1×10^7) from 9- to 10-week-old BALB/c mice were transferred intravenously into BALB/c *nu/nu* mice. The following day, anti-CD3 antibody was injected intraperitoneally. Small intestines were removed at 4 and 24 h after the injection and prepared for histological analysis. In the dual-grafting experiment, donor SPL (5×10^7) and IEL (1×10^7) were successively engrafted into BALB/c *nu/nu* mice.

Experiment 2. Freshly isolated IEL (1×10^7) from 6- to 11-week-old BALB/c mice were transferred intravenously into BALB/c *nu/nu* mice. After 5 weeks, anti-CD3 antibody was injected intraperitoneally. In the dual-grafting experiment,

donor SPL (5×10^7) were engrafted at 24 h before the anti-CD3 antibody injection.

Statistical analysis

Statistical comparisons were made using Scheffe's method after analysis of variance. The results were considered significantly different when $P < 0.05$. All analyses were carried out using StatView version 5.0 (SAS Institute Inc., Cary, NC, USA).

Results

Anti-CD3 antibody injection induces bi-phasic apoptosis in IEC

Anti-CD3 antibody induced apoptosis in many IEC in the small intestinal villus and crypts in a bi-phasic manner (i.e. early and late) (Figs 1–3). In the first phase, apoptosis of ciliated villous IEC with condensed nuclei (Figs 2B, D, G and 3A) began to appear at 2 h after the injection, peaked at 4 h and declined thereafter (Fig. 1A). The intestine showed villous shortening and a decline in the number of IEC (Fig. 2C). In the second phase, apoptosis of crypt IEC (Figs 2C, E, H and 3B) increased gradually for 24 h. In addition to H&E staining, TUNEL staining (Fig. 2G and H) and electron microscopic findings (Fig. 3) at 4 and 24 h clearly showed that both phases of apoptosis were induced mainly in IEC, although TUNEL-positive cells were also observed in the lamina propria from 2 to 24 h. Apoptotic bodies in the villus and the crypt decreased to normal levels by days 3 and 4, respectively (data not shown). A low level of crypt hyperplasia and villous atrophy was observed at 4 h and markedly from 24 to 48 h. Inflammatory infiltrates of mononuclear cells were noted in the lamina propria at day 2, but the histological features returned almost to normal by day 4 (data not shown). Apoptotic bodies increased dose dependently, reaching a plateau at a dose of 12.5 μg per mouse in the villus at 4 h and 6.3 μg per mouse in the crypt at 24 h (Fig. 1B and C). Therefore, all further experiments were performed using a dose of 12.5 μg CD3 antibody per mouse. The administration of control hamster IgG1κ had no effect on IEC apoptosis levels or histology (data not shown).

Apoptosis in IEC is induced by anti-CD3 via Fas/FasL interactions in vivo

IEC constitutively express Fas (11, 26), and IEL exert potent Fas-mediated killing activity after *in vitro* CD3 stimulation (27). To investigate whether Fas is involved in the apoptosis observed here, we used the Fas-deficient strain, MRL-*lpr/lpr* (Fig. 4). In MRL-+/+, normal Fas-expressing mice, bi-phasic apoptosis was induced by anti-CD3 injection to the same level as observed in C3H/HeN. On the other hand, in MRL-*lpr/lpr*, apoptosis in both phases was markedly reduced. These results suggest that the Fas/FasL system mediates a large portion of the observed apoptosis.

The *in vivo* administration of anti-CD3 may result in the stimulation of different types of T lymphocytes. Therefore, to clarify which T cell compartments, IEL, PPL, MLNC and SPL, were activated and presented cytotoxicity by the anti-CD3

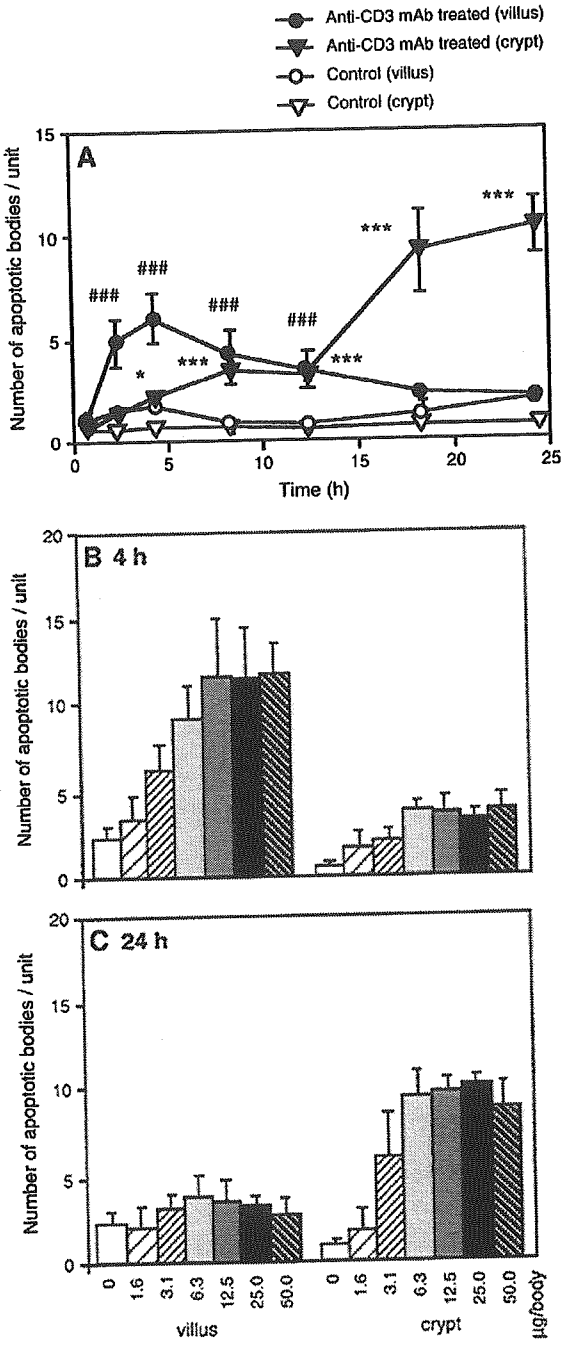

Fig. 1. Time course (A) and dose dependency (B, C) of anti-CD3-induced apoptosis in the jejunum of C3H/HeN mice. Control mice received saline alone. Data represent the means ± SD of apoptosis per villus per crypt unit. (A) The antibody was administered intraperitoneally at a dose of 12.5 μg per mouse (number of mice = 6–7). Apoptotic cells with condensing/fragmenting nuclei appeared in the small intestine bi-phasically. ### $P < 0.0005$ versus the control group (villus) and *$P < 0.05$; ***$P < 0.0005$ versus the control group (crypt) at each time. (B) Four hours after and (C) 24 h after antibody injection (number of mice = 5). Apoptotic cells with condensing/fragmenting nuclei arose dose dependently in the villus at 4 h (B) and in the crypt at 24 h (C).

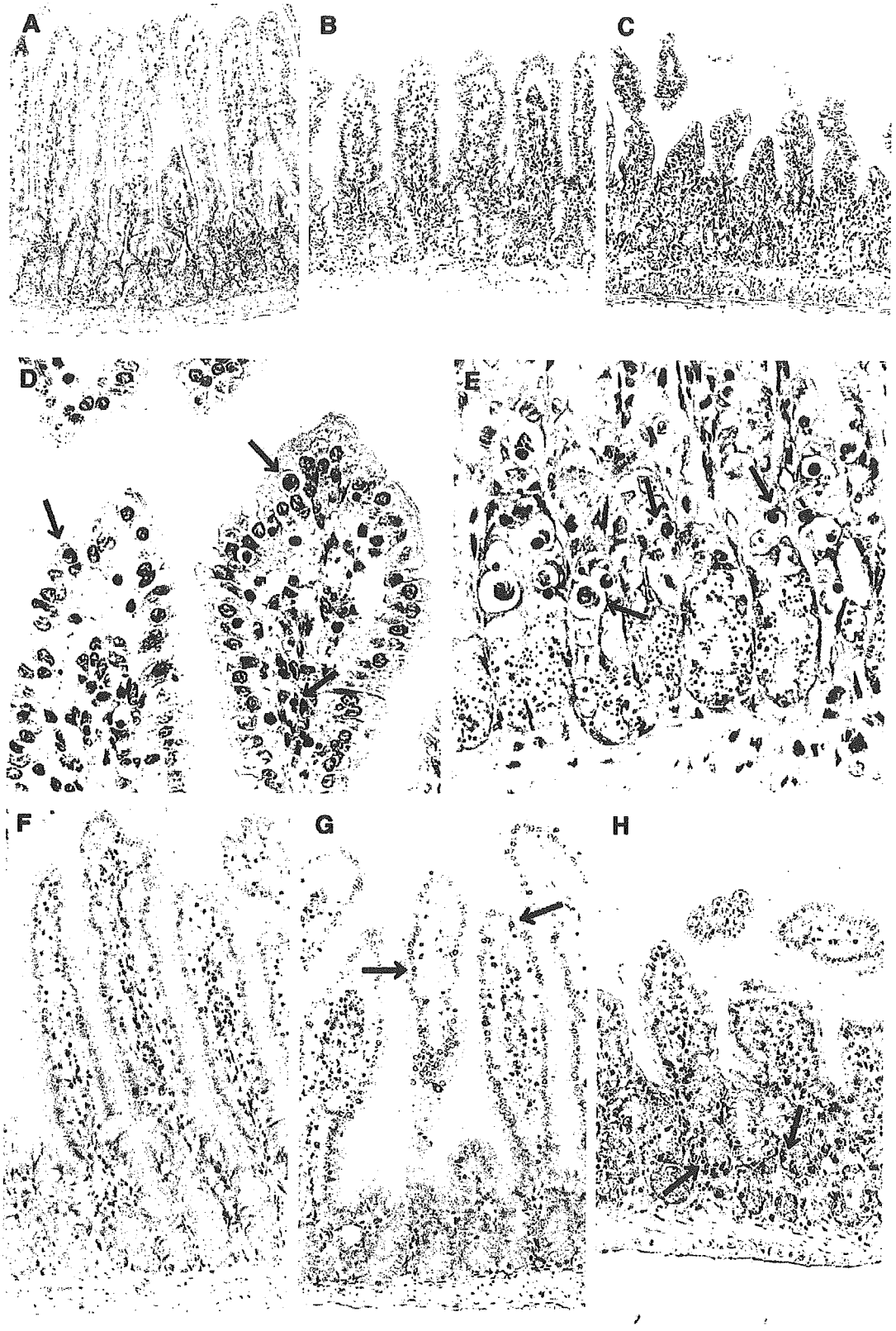
A
B
C
D
E
F
G
H

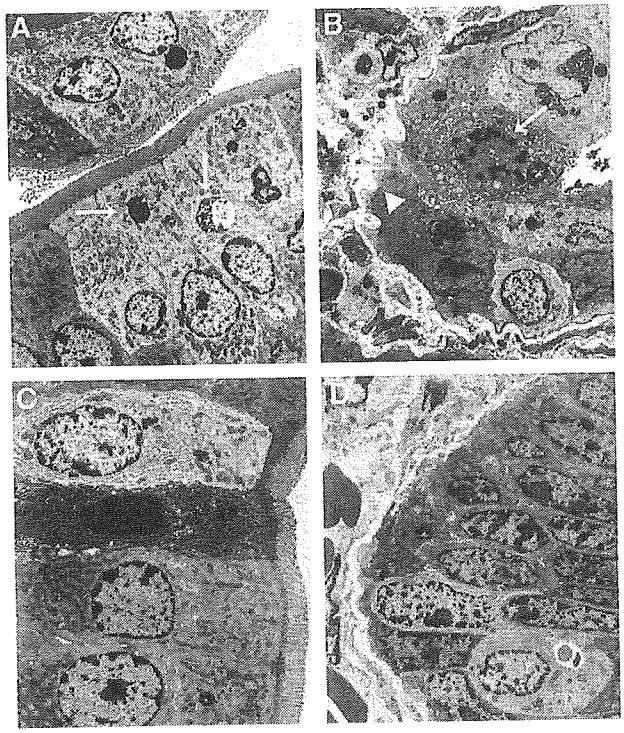

Fig. 3. Electron microscopic findings after anti-CD3 injection. (A) Condensed and fragmented nuclei (arrow) are seen in ciliated villous epithelial cells 4 h after anti-CD3 injection. The cytoplasm shows little change at this time. Neither apoptotic nor damaged lymphocyte infiltrate is observed. Little apoptosis occurs in IEL (unpublished observations in our laboratory). (B) Condensed and fragmented nuclei (arrow) and expanded mitochondria are seen in one crypt epithelial cell 24 h after anti-CD3 injection. The other crypt epithelial cells do not have typical condensed and/or fragmented nuclei, but nuclei are beginning to show damage. Neither apoptotic nor damaged lymphocyte infiltrate is present. The arrowhead indicates basal membrane. Little apoptosis occurs in lamina propria lymphocytes (unpublished observations in our laboratory). (C) Villus in naive mice and (D) crypt in naive mice. Naive mice have little apoptosis either in the villus or the crypt. The invasion of any microflora has not been observed in the small intestinal epithelia (A–D and unpublished observations). Original magnification: ×50 000.

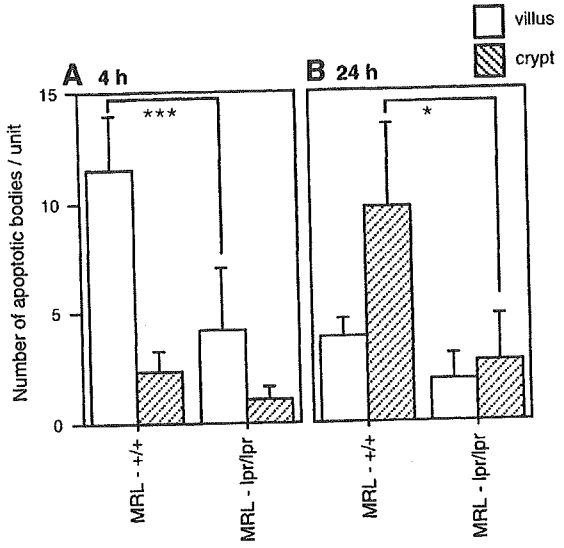

Fig. 4. Differences in the number of apoptotic cells in MRL-+/+ and MRL-*lpr/lpr* mice after anti-CD3 (12.5 μg per mouse) administered intraperitoneally. Apoptotic bodies with clearly fragmented and/or condensed nuclei, the most classical and definitive feature of apoptosis, were counted as described in *Histology* in Methods. Data represent the means ± SD of apoptotic cells per villus per crypt unit 4 (A) and 24 h (B) after antibody administration (number of mice = 3–5). The number of apoptotic bodies in mice administered saline instead of anti-CD3 was <1.5 for both strains. $*P < 0.05$; $***P < 0.0005$ versus the control group.

injection accompanied by intestinal injury, we analyzed *ex vivo* Fas-mediated cytotoxicity of these lymphocytes after anti-CD3 injection. At an E/T ratio of 1 : 20, freshly isolated IEL and SPL showed a weak spontaneous killing activity, with IEL stronger than SPL, but MLNC and PPL showed no detectable activity (Fig. 5A). When stimulated with anti-CD3 *in vitro*, cytotoxicity mediated by IEL and SPL was strongly induced, but was only marginally induced in MLNC and PPL, which is consistent with the data of Lin *et al.* (23) (Fig. 5B). Next, we analyzed the killer activity of lymphocytes isolated from mice injected with anti-CD3 antibody without *in vitro* stimulation (Fig. 5C). Similar to cells stimulated *in vitro*, the *in vivo* induction of cytotoxicity by anti-CD3 was mainly observed in IEL and SPL. The cytotoxicity of IEL increased rapidly and remained at the highest level from 0.5 to 4 h after the anti-CD3 injection and, thereafter, declined slowly. In contrast, SPL cytotoxicity rose more slowly, peaked from 4 to 8 h after the injection and then declined. The maximum cytotoxicities of IEL and SPL were similar to the maximum value obtained by *in vitro* stimulation, and the potency was IEL > SPL (approximately 60 versus 40% lysis at an E/T ratio of 1 : 20). The killer activity at 24 h was not analyzed because IEL were depleted by that time in this model. These results showed that the cytotoxicity of IEL and SPL was induced at different times and with different potency, which raised the possibility that IEL and SPL may be responsible for the induction of the different phases of IEC apoptosis.

We examined the expression of CD3, CD69, FasL and Fas on IEL and SPL from anti-CD3-treated and untreated mice (Fig. 6). FasL was constitutively expressed on IEL, but the number of $FasL^+$ cells increased slightly at 4 h after injection of anti-CD3 and returned to the normal levels by 24 h. On the other hand, FasL was expressed at a very low level on SPL of

Fig. 2. Histological sections of the jejunum of C3H/HeN mice. Anti-CD3 was administered at a dose of 12.5 μg per mouse. (A–E) H&E staining. (F–H) TUNEL assay. (A and F) Control mice receiving saline alone. (B, D and G) Four hours after the antibody injection. (C, D and G) Twenty-four hours after the antibody injection. Control mice have few apoptotic cells (A and F). Many apoptotic cells (arrow) are seen in the villus at 4 h (D and G) and in the crypt at 24 h (E and H) after anti-CD3 injection. Original magnification: A–C, ×25; D and E, ×132; F–H, ×50.

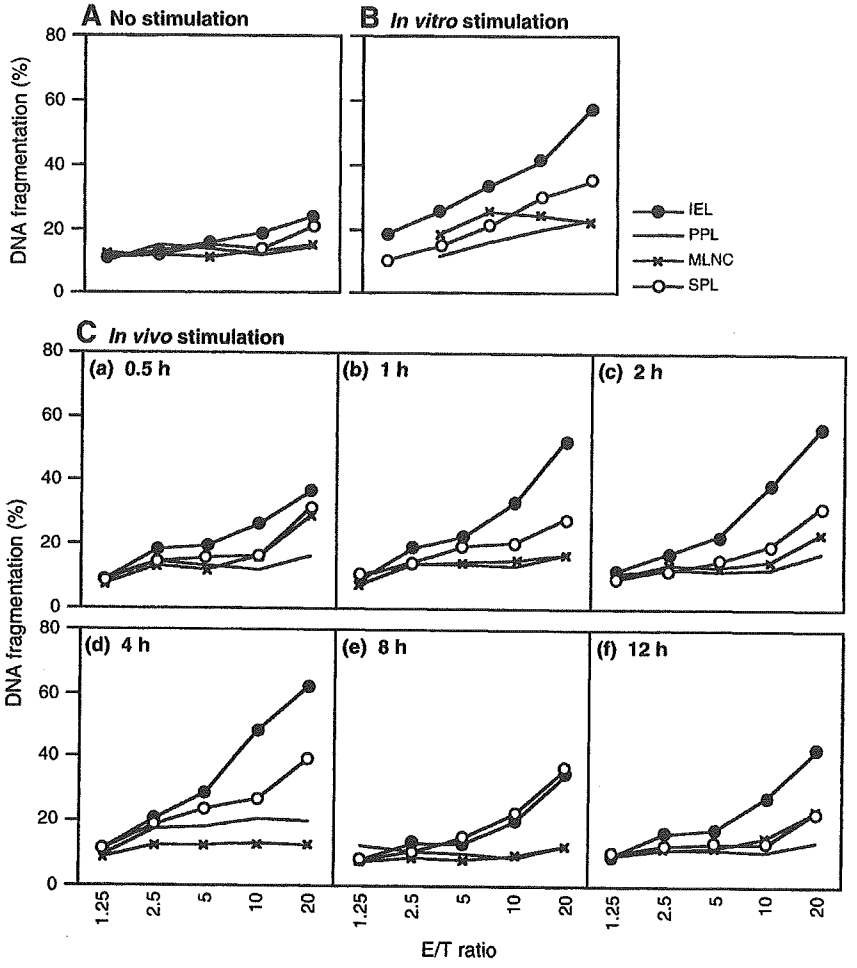

Fig. 5. Fas-mediated killer activity of lymphocytes. Lymphocytes isolated from naive C3H/HeN mice were cultured in the absence (A) or presence (B) of plate-bound anti-CD3 antibody. (C) Lymphocytes isolated from anti-CD3-injected C3H/HeN mice at different times after treatment were cultured in the absence of anti-CD3 antibody. Lymphocytes were pooled from three mice and a representative experiment of two performed is shown. The percentage of DNA fragmentation of Jurkat cells was measured and calculated as described in *Fas-mediated cytotoxicity assay* in Methods.

naive mice and increased at 4 and 24 h after the antibody injection. The number of $CD3^+$ cells and the density of CD3 expression on both IEL and SPL decreased at 4 h due to down-regulation of CD3, as previously reported (28–30). However, these values recovered by 24 h after the injection. Conversely, the amount of the activation marker, CD69, on both IEL and SPL was increased at 4 h after the injection and decreased to normal levels at 24 h, suggesting a rapid, temporary T cell activation.

Thymus-derived lymphocytes are involved in both phases of IEC apoptosis induced by anti-CD3

To directly confirm the involvement of thymus-derived T cells in the apoptosis observed here, we injected anti-CD3 into nude mice (Fig. 7). In euthymic BALB/c, the antibody induced bi-phasic apoptosis similar to that observed in C3H/HeN. By contrast, in athymic nude mice, both phases of apoptosis were almost completely abrogated, being depressed to the same levels as observed in normal BALB/c that were not administered antibody.

Adoptive transfer reconstitutes IEC apoptosis in nude mice

These data suggested the following hypotheses: the first phase of apoptosis at 4 h after the injection was induced by thymus-derived IEL, and the second phase at 24 h was induced by peripheral lymphocytes. To test these hypotheses, we adoptively transferred SPL or IEL isolated from euthymic mice into nude mice at 1 day before the anti-CD3 injection (Fig. 8, experiment 1). Transfer of SPL followed by anti-CD3 resulted in a substantial reconstitution of the second phase of apoptosis with crypt hyperplasia without villous apoptosis/destruction (Fig. 8, experiment 1B). However, neither phase of apoptosis was induced by the antibody in mice into which IEL had been transferred (Fig. 8, experiment 1). In addition, we adoptively transferred SPL and IEL successively, then administered anti-CD3. Unexpectedly, dual grafting of SPL

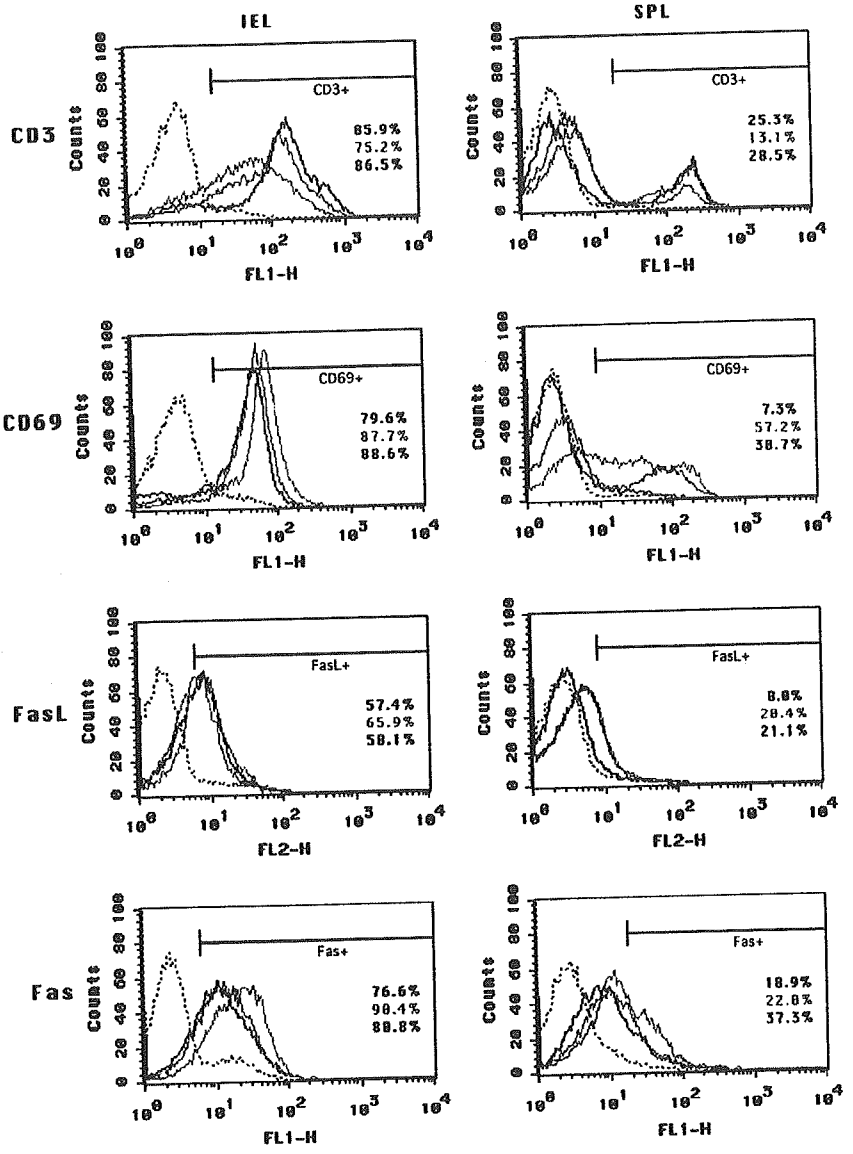

Fig. 6. Expression of CD3, CD69, FasL and Fas on IEL and SPL. Lymphocytes were isolated from naive (black line) or anti-CD3-treated C3H/HeN mice 4 (red line) and 24 (blue line) h after the injection and pooled from three mice. A representative experiment of the three performed is shown. The dotted line represents the isotype control. Numbers indicate the percentages of positive cells.

and IEL from euthymic mice induces neither the first phase nor the second phase of apoptosis in nude mice (Fig. 8, experiment 1B).

In experiment 2, because the migration of transferred IEL into the intestinal epithelium has been reported to take more than several weeks (31, 32), we changed the timing of IEL transfer. We adoptively transferred IEL, and after 5 weeks, the anti-CD3 antibody was injected (Fig. 8, experiment 2). IEL transfer significantly induced not only the first phase of apoptosis at 4 h (Fig. 8, experiment 2A) but also the second phase of apoptosis at 24 h after the anti-CD3 injection (Fig. 8, experiment 2B). Further, substantial apoptosis was detected in the villus at 24 h, which had not been so prominent in anti-CD3 antibody-treated euthymic BALB/c mice. Finally, differing from the results of experiment 1, dual grafting of SPL and IEL showed additive effects on IEC apoptosis (Fig. 8, experiment 2).

In the transfer experiments without anti-CD3 injection, no aberrant morphological changes were observed and no aberrant IEC apoptosis occurred following adoptive transfer of IEL, SPL or both (data not shown).

Discussion

In the present study, the following results were obtained: (i) anti-CD3 injections induced the apoptosis of small intestinal IEC bi-phasically with different spatial and temporal patterns,

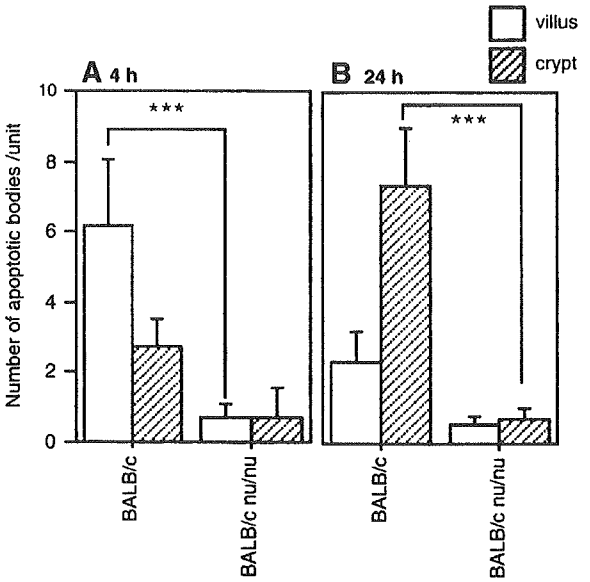

Fig. 7. Differences between the number of apoptotic cells in BALB/c and BALB/c *nu/nu* mice after intraperitoneal anti-CD3 (12.5 μg per mouse) administration. Apoptotic bodies with clearly fragmented and/or condensed nuclei, the most classical and definitive feature of apoptosis, were counted as described in Methods. Data represent the means ± SD of apoptotic cells per villus per crypt unit 4 (A) and 24 h (B) after antibody administration (number of mice = 4). The number of apoptotic bodies in mice administered with saline instead of anti-CD3 was <1.5 for both strains. The experiment was repeated three times with similar results. ***$P < 0.0005$.

(ii) each phase of apoptosis depended on Fas/FasL, (iii) anti-CD3 induced Fas-dependent cytotoxicity mediated by IEL rapidly, and by SPL gradually, (iv) each phase of apoptosis depended on thymus-derived T cells, (v) the adoptive transfer of SPL from euthymic mice to nude mice reconstituted only the second phase of IEC apoptosis, (vi) the adoptive transfer of IEL reconstituted both phases of IEC apoptosis, when anti-CD3 antibody was administered at 5 weeks after IEL transfer and (vii) dual grafting of SPL and IEL showed either abrogative or additive effects on IEC apoptosis, depending on the engrafting protocol.

A few studies have characterized the pathology and pathogenesis of anti-CD3 antibody-induced small intestinal lesions (33, 34). Merger *et al.* (17) demonstrated that multiple pathways of cytotoxicity, including tumor necrosis factor-α (TNF-α)-, Fas/FasL-, and perforin-mediated apoptosis, were associated with architectural damage. We have employed a model of enteropathy induced by a protocol similar to theirs, but some different results were obtained. Our data demonstrated that the antibody-induced bi-phasic apoptosis differed in spatiotemporal distribution, which was not previously noted. In addition, in our study, Fas/FasL-mediated killing played a major role in T cell-induced mucosal damage, whereas Merger *et al.* (17) indicated that the absence of Fas/FasL did not reduce apoptosis. This discrepancy may be due to differences in the dose of antibody used. In various studies, antibody was injected intravenously at relatively high doses (from 50 to 400 μg per mouse), whereas we used a dose of 12.5 μg per mouse intraperitoneally (17, 33, 34). At this dose, the number of apoptotic cells had already reached the maximum value (Fig. 1B and C). However, we also observed that the intestinal tissue damage that developed in our experimental setting was milder and recovered more rapidly than that at higher antibody doses (data not shown). Further, in contrast to previous studies, serum TNF-α was not detected at any time point up to 24 h after the injection (data not shown; detection limit: 50 pg ml^{-1}). These data suggest that the Fas/FasL pathway is important for the T cell-mediated IEC apoptosis following a weaker stimulation by anti-CD3 and that higher doses of the antibody stimulate various additional immunological responses and result in more complicated, long-term and serious enteropathy. Nonetheless, other cytotoxic pathways, for example perforin, suggested to be a very important cytotoxic pathway by Merger *et al.* (17), may contribute to IEC apoptosis in the present study because it was incompletely inhibited in the absence of Fas (in *lpr/lpr* mice). Thus, our protocol may be useful to discriminate and analyze the involvement of different cytotoxic mechanisms causing intestinal damage.

In the present study, in addition to the analysis using *lpr/lpr* mice, we quantified the Fas-mediated killing activity of lymphocytes from different compartments isolated from mice administered anti-CD3 antibody and found that the enhanced cytotoxicity of IEL and SPL was seen at different times. The enhanced killer activity of IEL and SPL at different times may, therefore, result in the induction of apoptosis at different times and sites. Complete abrogation of both phases of apoptosis in nude mice suggests an essential contribution of thymus-derived T cells. Indeed, αβIEL, which contain a large portion of thymus-derived T cells, showed stronger killer activity than γδIEL, which consist mainly of gut-derived T cells (data not shown). These data suggest the hypothesis that the first phase of apoptosis is mediated mainly by thymus-derived IEL and the second phase is mediated by peripheral lymphocytes. Lymphocyte transfer experiments provided data that were, at least partially, consistent with this hypothesis. Namely, the adoptive transfer of SPL from euthymic mice to nude mice before anti-CD3 injection resulted in only the second phase of apoptosis, whereas IEL caused both (Fig. 8). Compared with anti-CD3 antibody-induced apoptosis in euthymic mice, the apoptosis induced in IEL-engrafted nude mice was more prominent in the villus at 24 h (Figs 7 and 8, experiment 2). This discrepancy remains to be clarified in the future, but the following should be considered. The rapid massive villous apoptosis induced in euthymic mice resulted in an extensive loss of intestinal villus by 24 h and, therefore, the number of observable villous apoptotic bodies may have decreased. A relatively longer villus (i.e. greater integrity) was observed in the intestine of dual-grafted nude mice (data not shown).

The concomitant transfer of IEL and SPL abrogated the SPL-induced second phase of apoptosis, but SPL transfer at 5 weeks after IEL transfer had an additive effect on the second phase of apoptosis at 24 h (Fig. 8). Clarification of this discrepancy also requires further investigation but may be explained by the following. In experiment 1, a substantial amount of transferred IEL may have accumulated in the spleen because the cells did not have sufficient time to repopulate

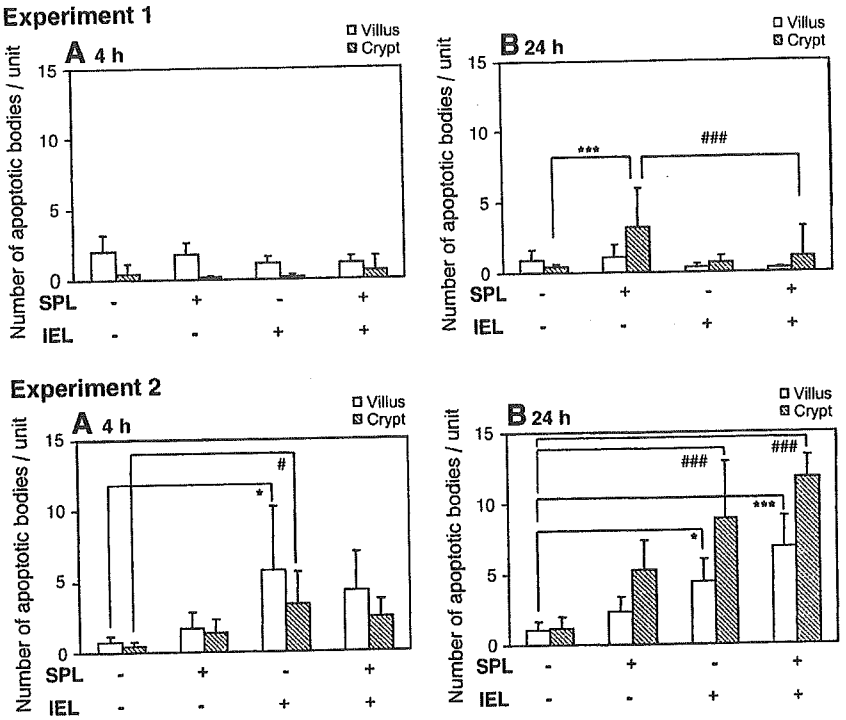

Fig. 8. Adoptive transfer of BALB/c IEL and SPL into BALB/c *nu/nu* mice. Experiment 1: naive nude mice were respectively or serially injected with SPL (5×10^7) and IEL (1×10^7). The day after the transfer, anti-CD3 was administered at a dose of 12.5 μg per mouse. The number of apoptotic cells 4 (A) and 24 h (B) after antibody administration is shown (number of mice = 5–13). The experiment was repeated twice with similar results. When SPL and/or IEL were transferred into the mice without anti-CD3 administration, the number of apoptotic bodies was <1.5 for all graft groups. Data represent means ± SD per villus per crypt unit. $***P < 0.0005$ versus non-transferred in crypt; $###P < 0.0005$ versus SPL transferred alone in crypt. Experiment 2: IEL (1×10^7) from 6- to 11-week-old-BALB/c mice were transferred to BALB/c *nu/nu* mice of the same age. After 5 weeks, saline or SPL (5×10^7) was transferred to the IEL-grafted or naive BALB/c *nu/nu* mice, and on the next day anti-CD3 was administered at a dose of 12.5 μg per mouse. The number of apoptotic cells 4 (A) and 24 h (B) after antibody administration is shown (number of mice = 5–6). When SPL and/or IEL without anti-CD3 administration were transferred to the mice, the number of apoptotic bodies was <1.5 for all graft groups. Data represent means ± SD per villus per crypt unit. $*P < 0.05$ and $***P < 0.0005$ versus non-transferred in the villus; $#P < 0.05$ and $###P < 0.0005$ versus non-transferred in the crypt.

the intestinal epithelium. In such a case, upon CD3 activation, $FasL^+$IEL may kill Fas^+SPL, including dendritic cells, which would result in the suppression of any T cell activation. By contrast, in experiment 2, many of the transferred IEL will have migrated into the intestine by 5 weeks after transfer, and therefore, the killing of SPL by IEL in the spleen may not occur when anti-CD3 antibody is injected. The killer activity of both IEL and SPL can thus be expressed additively, resulting in the observed enhanced killing of IEC.

It has been reported that 78.9% of IEC express the Fas molecule and the expression is not uniform (11). In addition, the sensitivity of cell death may be different between the villus and crypt because P53-independent cell death occurred by ischemia-reperfusion is induced in the villus to a greater extent than in the crypt (20). One explanation for bi-phasic apoptosis may be that villous IEC is more sensitive than crypt IEC for FasL signaling. The differences in the sensitivity of IEC to apoptosis may contribute to the bi-phasic apoptosis when mediated by IEL, especially. However, this hypothesis appears unsatisfactory because it does not provide a full explanation of the data presented in Figure 8, experiments 1 and 2, in that the anti-CD3-injection to SPL-grafting nude mice resulted in the second phase apoptosis only.

In summary, we have described a model of small intestinal injury induced by systemic T cell activation and characterized by IEC apoptosis with at least two distinct phases mediated mainly by the Fas/FasL system of thymus-derived T cells. Differential involvement of both peripheral and mucosal lymphocytes in the induction of the apoptosis has been demonstrated. Despite the many unresolved issues raised by these experiments, the demonstration of the possible involvement of different T cell compartments and their interactions in IEC apoptosis provides an important advance and useful tools in the effort to determine the components and mechanisms by which immune responses are regulated in normal and pathological intestinal mucosa.

Acknowledgements

The authors thank Dr Yasuhiro Komatsu, an ex-chief manager of Kampo & Pharmacognosy Laboratory of Tsumura & Co., for his valuable discussions.

Abbreviations

DEAE	diethylaminoethyl
E/T	Effecter/Target
FasL	Fas ligand
H&E	hematoxylin and eosin
IEC	intestinal epithelial cells
IEL	intestinal intraepithelial lymphocytes
MLNC	mesenteric lymph node cells
PPL	Peyer's patch lymphocytes
SPL	splenocytes
TNF	tumor necrosis factor
TUNEL	terminal deoxynucleotidyl transferase-mediated dUTP nick-end labeling

References

1 Fiocchi, C. 1998. Inflammatory bowel disease: etiology and pathogenesis. *Gastroenterology* 115:182.
2 Radford-Smith, G. 1997. Ulcerative colitis: an immunological disease? *Bailliere's Clin. Gastroenterol.* 11:35.
3 Schuppan, D. 2000. Current concepts of celiac disease pathogenesis. *Gastroenterology* 119:234.
4 Ueyama, H., Kiyohara, T., Sawada, N. *et al.* 1998. High Fas ligand expression on lymphocytes in lesions of ulcerative colitis. *Gut* 43:48.
5 Suzuki, A., Sugimura, K., Ohtsuka, K. *et al.* 2000. Fas/Fas ligand expression and characteristics of primed CD45RO+ T cells in the inflamed mucosa of ulcerative colitis. *Scand. J. Gastroenterol.* 35:1278.
6 Ciccocioppo, R., Di Sabatino, A., Parroni, R. *et al.* 2000. Cytolytic mechanisms of intraepithelial lymphocytes in coeliac disease (CoD). *Clin. Exp. Immunol.* 120:235.
7 Di Sabatino, A., D'Alo, S., Millimaggi, D. *et al.* 2001. Apoptosis and peripheral blood lymphocyte depletion in coeliac disease. *Immunology* 103:435.
8 Di Sabatino, A., Ciccocioppo, R., D'Alo, S. *et al.* 2001. Intraepithelial and lamina propria lymphocytes show distinct patterns of apoptosis whereas both populations are active in Fas based cytotoxicity in coeliac disease. *Gut* 49:380.
9 Ciccocioppo, R., Di Sabatino, A., Parroni, R. *et al.* 2001. Increased enterocyte apoptosis and Fas-Fas ligand system in celiac disease. *Am. J. Clin. Pathol.* 115:494.
10 Ciccocioppo, R., D'Alo, S., Di Sabatino, A. *et al.* 2002. Mechanisms of villous atrophy in autoimmune enteropathy and coeliac disease. *Clin. Exp. Immunol.* 128:88.
11 Sakai, T., Kimura, Y., Inagaki-Ohara, K., Kusugami, K., Lynch, D. H. and Yoshikai, Y. 1997. Fas-mediated cytotoxicity by intestinal intraepithelial lymphocytes during acute graft-versus-host disease in mice. *Gastroenterology* 113:168.
12 Bonhagen, K., Thoma, S., Leithauser, F., Moller, P. and Reimann, J. 1998. A pancolitis resembling human ulcerative colitis (UC) is induced by CD4+ TCR alphabeta T cells of athymic origin in histocompatible severe combined immunodeficient (SCID) mice. *Clin. Exp. Immunol.* 112:443.
13 Miwa, K., Hashimoto, H., Yatomi, T., Nakamura, N., Nagata, S. and Suda, T. 1999. Therapeutic effect of an anti-Fas ligand mAb on lethal graft-versus-host disease. *Int. Immunol.* 11:925.
14 Kataoka, Y., Iwasaki, T., Kuroiwa, T. *et al.* 2001. The role of donor T cells for target organ injuries in acute and chronic graft-versus-host disease. *Immunology* 103:310.
15 Arnold, D., Wasem, C., Juillard, P. *et al.* 2002. IL-18-independent cytotoxic T lymphocyte activation and IFN-gamma production during experimental acute graft-versus-host disease. *Int. Immunol.* 14:503.
16 Mowat, A. M. and Vinley, J. L. 1997. The anatomical basis of intestinal immunity. *Immunol. Rev.* 156:145.
17 Merger, M., Viney, J. L., Borojevic, R. *et al.* 2002. Defining the roles of perforin, Fas/FasL, and tumour necrosis factor alpha in T cell induced mucosal damage in the mouse intestine. *Gut* 51:155.
18 Tsuzuki, T., Yoshikai, Y., Ito, M., Mori, N., Ohbayashi, M. and Asai, J. 1994. Kinetics of intestinal intraepithelial lymphocytes during acute graft-versus-host disease in mice. *Eur. J. Immunol.* 24:709.
19 Okudela, K., Ito, T., Mitsui, H. *et al.* 1999. The role of p53 in bleomycin-induced DNA damage in the lung. A comparative study with the small intestine. *Am. J. Pathol.* 155:1341.
20 Coopersmith, C. M., O'Donnell, D. and Gordon, J. I. 1999. Bcl-2 inhibits ischemia-reperfusion-induced apoptosis in the intestinal epithelium of transgenic mice. *Am. J. Physiol.* 276:G677.
21 Pritchard, D. M. and Watson, A. J. 1996. Apoptosis and gastrointestinal pharmacology. *Pharmacol. Ther.* 72:149.
22 Taguchi, T., McGhee, J. R., Coffman, R. L. *et al.* 1990. Analysis of Th1 and Th2 cells in murine gut-associated tissues. Frequencies of CD4+ and CD8+ T cells that secrete IFN-gamma and IL-5. *J. Immunol.* 145:68.
23 Lin, T. S., Brunner, T., Tietz, B. *et al.* 1998. Fas ligand-mediated killing by intestinal intraepithelial lymphocytes—participation in intestinal graft-versus-host disease. *J. Clin. Investig.* 101:570.
24 Ramsdell, F., Seaman, M. S., Miller, R. E., Tough, T. W., Alderson, M. R. and Lynch, D. H. 1994. gld/gld mice are unable to express a functional ligand for Fas. *Eur. J. Immunol.* 24:928.
25 Yamamoto, M., Ogawa, K., Morita, M., Fukuda, K. and Komatsu, Y. 1996. The herbal medicine Inchin-ko-to inhibits liver cell apoptosis induced by transforming growth factor beta 1. *Hepatology* 23:552.
26 Yukawa, M., Iizuka, M., Horie, Y. *et al.* 2002. Systemic and local evidence of increased Fas-mediated apoptosis in ulcerative colitis. *Int. J. Colorectal Dis.* 17:70.
27 Inagaki-Ohara, K., Nishimura, H., Sakai, T., Lynch, D. H. and Yoshikai, Y. 1997. Potential for involvement of Fas antigen Fas ligand interaction in apoptosis of epithelial cells by intraepithelial lymphocytes in murine small intestine. *Lab. Investig.* 77:421.
28 Ellenhorn, J. D., Hirsch, R., Schreiber, H. and Bluestone, J. A. 1988. *In vivo* administration of anti-CD3 prevents malignant progressor tumor growth. *Science* 242:569.
29 Hirsch, R., Eckhaus, M., Auchincloss, H., Jr., Sachs, D. H. and Bluestone, J. A. 1988. Effects of *in vivo* administration of anti-T3 monoclonal antibody on T cell function in mice. I. Immunosuppression of transplantation responses. *J. Immunol.* 140:3766.
30 Hirsch, R., Gress, R. E., Pluznik, D. H., Eckhaus, M. and Bluestone, J. A. 1989. Effects of *in vivo* administration of anti-CD3 monoclonal antibody on T cell function in mice. II. *In vivo* activation of T cells. *J. Immunol.* 142:737.
31 Poussier, P., Edouard, P., Lee, C., Binnie, M. and Julius, M. 1992. Thymus-independent development and negative selection of T cells expressing T cell receptor alpha/beta in the intestinal epithelium: evidence for distinct circulation patterns of gut- and thymus-derived T lymphocytes. *J. Exp. Med.* 176:187.
32 Suzuki, S., Sugahara, S., Shimizu, T. *et al.* 1998. Low level of mixing of partner cells seen in extrathymic T cells in the liver and intestine of parabiotic mice: its biological implication. *Eur. J. Immunol.* 28:3719.
33 Ferran, C., Dy, M., Sheehan, K. *et al.* 1991. Inter-mouse strain differences in the *in vivo* anti-CD3 induced cytokine release. *Clin. Exp. Immunol.* 86:537.
34 Ferran, C., Dy, M., Sheehan, K. *et al.* 1991. Cascade modulation by anti-tumor necrosis factor monoclonal antibody of interferon-gamma, interleukin-3 and interleukin-6 release after triggering of the CD3/T cell receptor activation pathway. *Eur. J. Immunol.* 21:2349.

Available online at www.sciencedirect.com

SCIENCE DIRECT®

Gynecologic Oncology 97 (2005) 243–245

Gynecologic Oncology

www.elsevier.com/locate/ygyno

Case Report

Primary omental gestational choriocarcinoma ascertained by deoxyribonucleic acid polymorphism analysis

Kaoru Sakumoto*, Yutaka Nagai, Morihiko Inamine, Koji Kanazawa

Department of Obstetrics and Gynecology, Faculty of Medicine, University of the Ryukyus, Okinawa, Japan

Received 28 May 2004
Available online 1 February 2005

Abstract

Background. Abdominal choriocarcinoma is extremely rare. It is important to examine whether the disease is primary or metastatic and gestational or non-gestational.

Case. A 26-year-old nulli-gravid woman underwent laparoscopy for presumed ectopic pregnancy. The uterus, ovaries and fallopian tubes surrounded by hemoperitoneum were unremarkable. A hemorrhagic 7-cm-sized tumor was identified on the greater omentum and excised. Histology was consistent with choriocarcinoma. Analysis of human leucocyte antigen (HLA) gene polymorphism on deoxyribonucleic acid (DNA) demonstrated that tumor DNA contained both HLA locus antigens of patient and of her husband. Clinical remission was achieved with six courses of chemotherapy.

Conclusion. To our knowledge, this is the first reported case of choriocarcinoma that occurred primarily on the omentum ascertained to be of gestational origin by DNA polymorphism analysis.

Keywords: Choriocarcinoma; DNA polymorphism analysis; Omentum

Introduction

Primary abdominal gestational choriocarcinoma is an extremely rare malignancy [1,2]. When a patient with abdominal choriocarcinoma is encountered, it is clinically important to examine whether the disease developed primarily there or metastasized secondarily there from genital choriocarcinoma and whether the disease is of gestational origin or of non-gestational germ cell origin.

Case

A 26-year-old nulli-gravid woman presented to our hospital with low abdominal pain and genital bleeding, 7 weeks after her last menstrual period. She had a history of regular menstruation and married 1 year earlier. A urinary pregnancy test was positive, indicating her first pregnancy. Physical examination revealed rebound tenderness in the lower abdomen. Inspection with a bivalve vaginal speculum demonstrated a closed cervical os with bloody discharge. Transvaginal ultrasonography showed free cul-de-sac fluid with no intrauterine gestational sac. Non-clotting blood was obtained by culdocentesis. The serum human chorionic gonadotropin (hCG) level was 103,704 mIU/mL.

Laparoscopy, performed for a presumed diagnosis of aborted or ruptured ectopic pregnancy, disclosed the uterus and bilateral adnexa surrounded by hemoperitoneum. After suction of intraperitoneal blood (approximately 650 mL), the uterus, tubes and ovaries were visualized completely and confirmed to be entirely normal in appearance. No bleeding lesions or injuries were found on the peritoneal surface of the genital structures and the pelvic cavity. Laparoscopic observation turned to the upper abdominal cavity. A hemorrhagic, dark reddish friable tumor, measuring 7.0 ×

* Corresponding author. Department of Obstetrics and Gynecology, Faculty of Medicine, University of the Ryukyus, 207 Uehara, Nishihara-Machi, Nakagami-Gun, Okinawa, Japan. Fax: +81 98 895 1426.
E-mail address: sakumoto@med.u-ryukyu.ac.jp (K. Sakumoto).

0090-8258/$ - see front matter © 2004 Elsevier Inc. All rights reserved.
doi:10.1016/j.ygyno.2004.09.036

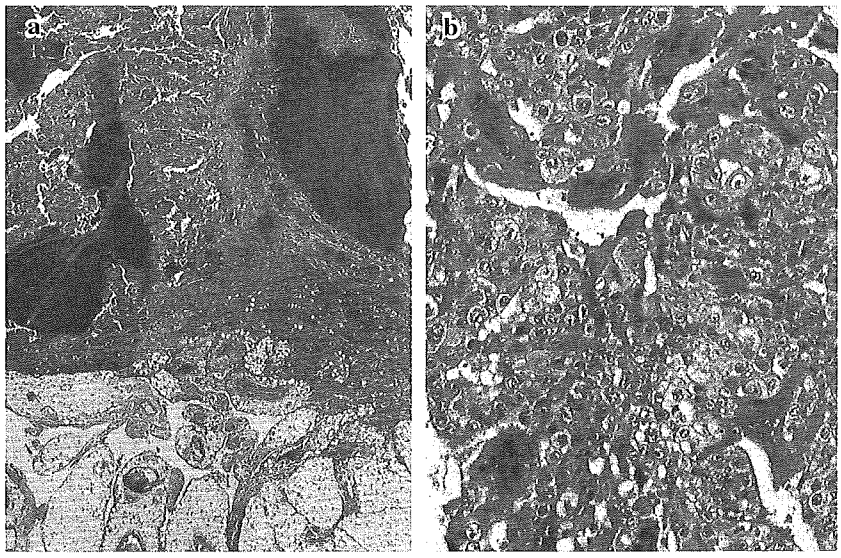

Fig. 1. Sheets and masses of tumor cells are seen in extensive hemorrhage and necrosis. On the bottom, the boundary with preserved omental fatty tissues circumscribes the tumor (a; hematoxylin–eosin, ×12). Cytotrophoblast, syncytiotrophoblast and intermediate trophoblast are present with no chorionic villi (b; hematoxylin–eosin, ×200).

5.0 × 4.5 cm, was seen on the right side surface of the greater omentum. The tumor was removed carefully along with the attached omental tissues under laparotomy. In addition, endometrial curettage was performed.

Histological examination of the resected tumor demonstrated a typical choriocarcinoma characterized by masses and sheets of markedly atypical trophoblastic cells with no component of chorionic villi, accompanied by extensive hemorrhage and necrosis (Fig. 1). No gestational tissues were noted in the endometrial specimen. Analysis of human leucocyte antigen (HLA) DRB gene polymorphism on deoxyribonucleic acids (DNAs) from tumor tissue, patient's leucocyte and her husband's leucocyte demonstrated that the tumor DNA contained both HLA DRB gene locus antigens of patient and of her husband (Fig. 2).

Her postoperative recovery was uneventful and serum hCG level declined to 350 mIU/mL 3 weeks later. No pulmonary or other distant metastases developed. Chemotherapy was given with a combination of methotrexate, actinomycin D and cyclophosphamide. Clinical remission was achieved with four courses of chemotherapy that were followed by two additional courses after normalization of hCG level. She has been healthy over 10 years with two healthy children.

Discussion

Recently, two interesting cases of abdominal extragenital or heterotopic gestational choriocarcinoma were reported. Bailey et al. [1] described a case of gestational choriocarcinoma occurring primarily on the left anterior abdominal wall of the pelvis, and Chen et al. [2] reported a case of gestational choriocarcinoma occurring primarily on the surface of subserosal uterine leiomyoma. They demonstrated that these

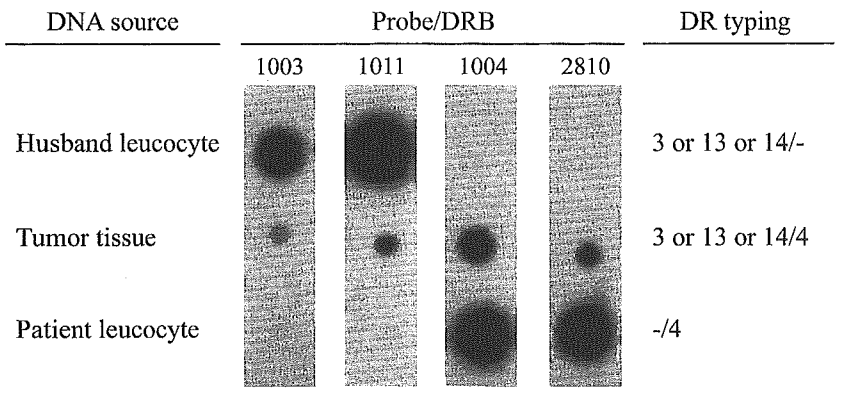

Fig. 2. Polymerase chain reaction-dot blot analysis with sequence-specific oligonucleotides targeted to the HLA DRB gene yielded the definite typing of tumor, patient and her husband.

cases were choriocarcinomas 'primarily' occurring at the disease sites, based on the appearance of the intact uterus or uterine cavity, tubes and ovaries free from pregnancy- or trophoblastic-tumor-associated findings. Our case also appears to be choriocarcinoma 'primarily' developing on the omental surface because of the same findings as those observed in their cases.

It is important to ascertain the mode of origin of choriocarcinoma because chemotherapy selection is contingent upon whether the tumor is of gestational versus non-gestational derivation. For example, it is described that gestational choriocarcinoma has a significantly better therapeutic response and prognosis than does non-gestational ovarian choriocarcinoma [3]. The authors of two previous case reports suggested that their cases were 'of gestational origin' arising from a conceptus in newly developed pregnancy, based on the patient's history of pregnancy signs after a missed normal menstrual period. Their suggestion seems to be reasonable, furthermore because nongestational choriocarcinoma is a rare malignant teratoid tumor that occurs mainly in the ovary of prepubescent children or adults younger than 20 years of age and that is usually admixed with other germ cell tumor elements, such as dysgerminoma, teratoma or yolk sac tumor [4,5]. In our case, an analysis of HLA gene polymorphism demonstrated that the tumor contained the allele from the patient's husband in addition to her allele, indicating the possibility that the tumor is of gestational origin, and not of parthenogenetic origin [6].

Although gestational choriocarcinoma is usually recognized following the sequel of such other trophoblastic products of conception as hydatidiform mole, abortion and pre-term or term pregnancy, it is described that primitive previllous trophoblasts may alternate directly with malignant trophoblasts [7]. Acosta-Sisson [8] termed such a case "choriocarcinoma ab initio" and cited clinical observations suggesting the existence of such a pathogenetic course. On the other hand, Friedrich [9] reported primary omental pregnancy, although it probably resulted from regurgitation and migration of an ovum that was fertilized in the tube. Thus, our case seems to be gestational choriocarcinoma that arose immediately from early-stage trophoblasts of a new conceptus that was implanted on the omentum. To our knowledge, this is the first reported case of choriocarcinoma that occurred primarily on the surface of the greater omentum and that was ascertained to be of gestational origin by HLA polymorphism analysis of tumor tissue.

Acknowledgment

The authors thank Professor Norio Wake (Department of Reproductive Physiology and Endocrinology, Kyushu University) for his kind assistance with outstanding study on DNA polymorphism analysis.

References

[1] Bailey JL, Hinton EA, Ashfaq R, Schorge JO. Primary abdominal gestational choriocarcinoma. Obstet Gynecol 2003;102:988–90.
[2] Chen M-J, Yang J-H, Lin M-C, Ho H-N, Yang Y-S. An unusual gestational choriocarcinoma occurring primarily on the surface of a subserous leiomyoma. Br J Obstet Gynaecol 2004;111:188–90.
[3] Dehner LP. Gestational and nongestational trophoblastic neoplasia: a historic and pathobiologic survey. Am J Surg Pathol 1980;4: 43–58.
[4] Nogales FF. Germ cell tumours of the ovary. In: Fox H, Wells M, editors. Haines and Taylor obstetrical and gynecological pathology, fourth ed. New York: Churchill Livingstone, 1995. p. 861–2.
[5] Talerman A. Germ cell tumors of the ovary. In: Kurman RJ, editor. Blaustein's pathology of the female genital tract, fifth ed. New York: Splinger-Verlag, 2002. p. 992–4.
[6] Arima T, Imamura T, Sakuragi N, Higashi M, Kamura T, Fujimoto S, Nakano H, Wake N. Malignant trophoblastic neoplasms with different modes of origin. Cancer Genet Cytogenet 1995;85:5–15.
[7] Hertz R. Spectrum of gestational trophoblastic disease. In: Hertz R, editor. Choriocarcinoma and related gestational trophoblastic tumors in women. New York: Raven Press, 1978. p. 13–22.
[8] Acosta-Sisson H. Can the implanting trophoblasts of the fertilized ovum develop immediately into chorionepithelioma? Am J Obstet Gynecol 1955;69:442–6.
[9] Friedrich MA. Primary omental pregnancy: 2 cases of primary peritoneal pregnancy. Obstet Gynecol 1968;31:104–9.

J. Perinat. Med. 33 (2005) 199–205 • Copyright © by Walter de Gruyter • Berlin • New York. DOI 10.1515/JPM.2005.037

Original articles – Obstetrics

Cerebral edema on MRI in severe preeclamptic women developing eclampsia

Hideo Matsuda*, Kenichiro Sakaguchi, Tomoko Shibasaki, Hironori Takahashi, Yuichi Kawakami, Kenichi Furuya and Yoshihiro Kikuchi

Department of Obstetrics and Gynecology, National Defense Medical College, Japan

Abstract

Objective: The aim of this study is to identify suitable applications for cerebral MR (magnetic resonance) scanning in cases of severe preeclampsia and eclampsia through comparison of clinical course and easily accessible parameters.

Methods: From January 2001 to December 2003, cerebral MR scans were performed on 43 women with severe preeclampsia; of those 41 were enrolled in data analyses. Twenty clinical parameters, including age, body mass index, blood pressure, liver and renal function, and coagulation status, were compared for each patient. Data were analyzed using the SPSS program on a VAX main frame.

Results: Among 41 severe preeclamptic women, abnormal MR images were observed in 11 cases including six with systemic seizures. Predictive accuracy of eclampsia with abnormal cerebral MR imaging was 84.9% ($P=0.00001$), while only 14.3% of severe preeclampsia cases had been diagnosed radiologically. Statistical analysis suggests diastolic BP and serum AST as predictive parameters for abnormal MR images with 82.9% predictive accuracy ($P=0.0007$).

Conclusions: Cerebral edema can be observed in preeclamptic patients developing eclampsia. Rapid delivery is indicated when diastolic BP and AST are elevated. MR scanning is useful when delivery is delayed due to fetal immaturityin cases of severe preeclampsia.

Keywords: Cerebral edema; eclampsia; MRI; posterior leukoencephalopathy; preeclampsia; pregnancy induced hypertension.

*Corresponding author:
Hideo Matsuda, MD
Department of Obstetrics and Gynecology
National Defense Medical College
3–2 Namiki, Tokorozawa
Saitama Prefecture
359-1513 Japan
Tel.: +81-42-995-1687
Fax: +81-42-996-5213
E-mail: hmatsuda@ndmc.ac.jp

Introduction

Eclampsia is defined as the new onset of convulsions during pregnancy or postpartum, unrelated to other cerebral pathologic conditions, in women with preeclampsia. Matter and Sibai [11] concluded that eclampsia remains a significant complication of pregnancy with high maternal mortality and morbidity rates, and that antepartum onset carries greater risks, with onset under 32 weeks' gestation being particularly dangerous to both mother and fetus. Thus, to predict the onset of eclampsia and start appropriate treatment as early as possible is important for favorable perinatal prognosis.

Brain magnetic resonance (MR) scans and MR angiographies are now widely used in various fields of clinical medicine, especially for hypertension, renal failure, and immunosuppressive medicine users. Reversible posterior leukoenchephalopathy is a typical finding in these patients, and it is also frequently observed in eclampsia patients. Weingarten [18] reported abnormal MR images in women with hypertensive encephalopathy including focal white matter lesions on the reversible generalized cerebral edema. Peterkin [14] reported that reversible cerebral MR abnormal images may be observed in severe preeclamptic women. However, these reports did not discuss when MR images should be taken, what clinical parameter is most reflective of maternal brain abnormality, or whether abnormal images always exist prior to the onset of eclampsia. Rutherford and colleagues [15] have studied the use of cerebral MRI in preeclampsia and concluded that it was not clinically useful when used routinely. MR scanning is an expensive imaging modality that requires patients to leave the area of care for a significant length of time and should therefore not be undertaken lightly.

This study was conducted in order to identify accessible clinical parameters for abnormal brain MR imaging in severe preeclampsia cases, and to identify appropriate applications for MR scanning in managing severe preeclampsia and eclampsia.

Methods

From January 1, 2001 to December 31, 2003, 92 patients with severe preeclampsia, as diagnosed under the guidelines of the National High Blood Pressure Education Program [13], were hospitalized and treated. Of those, 43 agreed to participate in

this study, and 2 subsequently dropped out because of their inability to undergo MR scanning due to claustrophobia. The remaining 41 were enrolled in data analyses. Magnesium sulfate prophylaxis (as per the Magpie trial [10] was used with all of these patients, and some were carefully treated with alpha methyldopa, labetalol hydrochloride, and calcium channel blockers such as nicardipine hydrochloride to await fetal maturation.

Maternal MR scans were performed on all patients without regard to headaches and visual symptoms in those with severe preeclampsia, and clinical data were recorded prior to MR scanning. Follow-up MR scans were repeated until the abnormal findings disappeared. Twenty clinical parameters, including age, body mass index, blood pressure, liver function, renal function, and coagulation status, were recorded for each patients. Magnetom Vision (Siemens, Germany) MR systems providing fluid-attenuated inversion recovery (FLAIR) sequences and diffusion-weighted images (DWI), were used. In DWI, calculation of apparent diffusion coefficient (ADC) map assessed the relationship between the diffusion constant from b-value of 0 s/mm^2 to b-value of 1000 s/mm^2, and b-value of 1000 s/mm^2 was specified as a measure of the diffusion sensitivity. Simultaneously, three-dimensional (3D) time-of-flight MR angiography (TOF MRA) was also applied. Each MR image was diagnosed by at least two radiologists.

Data were analyzed using the SPSS program on a VAX main frame.

Correlation of eclampsia and abnormal brain MR images was calculated with a χ^2 test. An analysis of variance was performed in order to measure the variations between each of the parameters. Bonferroni tests comparisons were performed between the abnormal MR group and normal MR group, and between the eclampsia group and non-eclampsia group. The stepwise discriminant procedure was used in order to determine the relative contribution of each variable. Two clinical parameters, diastolic blood pressure (BP) and serum AST were subjected to both stepwise and direct discriminant analysis in order to calculate a specific discriminant formula. Expected abnormality detection with MRI was compared to the results of MR scanning with the χ^2 test.

Results

All 41 women were treated with magnesium sulfate prophylaxis on their admission to the National Defense Medical College Hospital. Among the 41 severe preeclampsia patients, six had systemic seizures (all of the patients with seizure had been transferred from local regional clinics), and 14 cases had visual symptoms without retinal detachmnet. Patients with systolic blood pressure over 180 mmHg and diastolic blood pressure over 120 mmHg were treated with one or two kinds of antihypertensive drugs, such as alpha methyldopa, labetalol hydrochloride, and calcium channel blockers, with careful fetal monitoring prior to MR scanning. Urinary protein of more than 3.5 g/day was observed in 12 cases. Abnormal MR images were obtained for 11 cases (nine of vasogenic edema and two of minor cerebral embolisms), the suspected vasoconstriction was observed in four cases. As shown in Table 1, of the 11 cases with abnormal MR findings, two cases developed eclampsia within 2 h of delivery, four cases developed eclampsia between 12 and 48 h postpartum, and five cases had no seizures. Typical abnormal MR images are shown in Figure 1, Figure 2, and Figure 3.

A 2×2 table of our MRI findings and eclampsia was performed and a specificity of 100.0%, sensitivity of 85.7%, positive predictive value of 54.5%, negative predictive value of 100.0%, and prediction accuracy of 87.8% ($P=0.00001$) were obtained (Table 2). For eclampsia, brain MR images showed some abnormality (especially posterior leukoencephalopathy) as has been reported elsewhere, while abnormal MR images were obtained for only 14.3% (5/35) of women with severe preeclampsia who had no seizures. This suggests that cerebral damage could exist prior to the onset of seizure in severe preeclampsia. Four women were thought to show vasoconstriction in 3D-TOF-MRA, but two of the four were possible anatomical variations.

Bonferroni analysis was performed to detect important, easily accessible clinical parameters for eclampsia (Table 3) and abnormal MR images (Table 4). Diastolic blood pressure (measured before MR scanning) and serum AST, ALT, LDH, and serum creatinine were observed to have statistical significance, while other parameters, such as systolic blood pressure, urine protein, uric acid, and antithrombin III, were not. We ascertained that diastolic blood pressure has more clinical significance than systolic blood pressure, and more significance in elevated liver enzymes than in renal malfunction and coagulopathy, in preventing eclampsia among severe preeclamptic patients, whereas all parameter were more severe than those for normal pregnant women. Although statistically significant differences were observed, differences between normal and abnormal measurements within each parameter were relatively small, thus making it possible to determine what parameter combinations would best predict MRI abnormalities. We therefore conducted stepwise discriminant analysis in order to identify the most predictive parameter combination.

A 2×2 table of expected MR abnormalities and actual abnormal MR diagnosis was calculated using stepwise discriminant analysis. After deriving an appropriate canonical coefficient, diastolic blood pressure and serum AST levels were selected. As shown in Table 5, this combination of parameters produced the best result statistically, with a prediction accuracy of 82.9% ($P=0.0007$). These two parameters were found to correlate with abnormal MR findings, although it is difficult to analyze the cut-off levels with these parameters with small data samples.

The time course of abnormal cerebral MR images is shown in Table 6. Prolonged elevated diastolic pressure and general fatigue were observed in case 1 and case 8, who suffered coma after seizures, and several MR scans were required to confirm "reversible" leukoencephalopathy. Rapid recoveries were observed after delivery in the remaining cases. 3D-TOF-MRA detected some sus-

Table 1 Characteristics of participants and MRI findings.

Case	Age	BP (mmHg)	UP (g/day)	Headaches	Visual symptoms	Seizures	MR diagnosis	Vasoconstriction
1	36	180/100	0.3	(+)	(+)	(+)	multi-lobal vasogenic edema, minimal infarction	suspected left ACA
2	31	170/120	18.2	(+)	(−)	(−)	posterior leukoencephalopathy	n.f.
3	35	180/122	0.3	(−)	(+)	(+)	basal ganglia vasogenic edema	n.f.
4	28	182/108	0.3	(+)	(+)	(+)	multi-lobal edema	right CA
5	29	163/120	0.1	(−)	(+)	(−)	n.f.	suspected right MCA
6	23	180/110	10.4	(−)	(+)	(+)	multi-lobal vasogenic edema, minimal infarction	n.f.
7	36	191/106	0.3	(+)	(+)	(+)	temporal and posterior leukoencephalopathy	n.f.
8	38	192/120	6.3	(+)	(+)	(−)	posterior encephalopathy	n.f.
9	28	180/110	1.7	(+)	(−)	(+)	multi-lobal edema	n.f.
10	38	170/100	10.0	(−)	(+)	(−)	n.f.	blt. ACA/PCA
11	32	170/110	7.6	(−)	(−)	(−)	basal ganglia vasogenic edema	n.f.
12	42	160/ 90	0.2	(−)	(+)	(−)	n.f.	n.f.
13	31	212/106	0.7	(−)	(+)	(−)	n.f.	n.f.
14	19	160/ 80	0.8	(−)	(+)	(−)	n.f.	n.f.
15	32	200/100	1.7	(−)	(+)	(−)	n.f.	n.f.
16	27	170/100	5.5	(−)	(+)	(−)	n.f.	n.f.
17	40	182/104	3.0	(−)	(−)	(−)	n.f.	n.f.
18	27	160/ 90	2.9	(−)	(−)	(−)	n.f.	n.f.
19	33	168/ 80	1.7	(−)	(−)	(−)	n.f.	n.f.
20	37	172/110	4.8	(−)	(−)	(−)	n.f.	n.f.
21	29	160/103	0.3	(−)	(−)	(−)	n.f.	n.f.
22	24	176/ 98	10.1	(−)	(−)	(−)	n.f.	n.f.
23	31	160/104	3.8	(−)	(−)	(−)	n.f.	n.f.
24	32	160/100	2.5	(−)	(−)	(−)	n.f.	n.f.
25	34	212/110	0.7	(−)	(+)	(−)	n.f.	n.f.
26	35	180/ 90	0.8	(−)	(−)	(−)	n.f.	n.f.
27	37	194/134	0.4	(−)	(−)	(−)	n.f.	n.f.
28	34	150/100	0.9	(−)	(−)	(−)	n.f.	n.f.
29	31	169/100	6.8	(−)	(−)	(−)	n.f.	n.f.
30	26	185/105	0.4	(−)	(−)	(−)	n.f.	n.f.
31	34	170/100	2.7	(−)	(−)	(−)	n.f.	n.f.
32	32	160/ 90	4.0	(−)	(−)	(−)	n.f.	n.f.
33	30	182/120	1.6	(−)	(−)	(−)	n.f.	n.f.
34	27	174/118	3.8	(−)	(−)	(−)	n.f.	n.f.
35	32	172/110	0.8	(−)	(−)	(−)	n.f.	n.f.
36	35	186/106	1.4	(−)	(−)	(−)	n.f.	n.f.
37	34	160/108	0.7	(−)	(−)	(−)	n.f.	n.f.
38	29	160/103	1.0	(−)	(−)	(−)	n.f.	n.f.
39	22	170/100	0.9	(−)	(−)	(−)	n.f.	n.f.
40	34	162/100	0.1	(−)	(−)	(−)	n.f.	n.f.
41	27	170/110	11.8	(−)	(−)	(−)	n.f.	n.f.

BP: Blood pressure prior to MR scans, UP: Urinary protein, n.f.: normal findings. ACA: anterior cerebral artery, CA: carotid artery, MCA: mid cerebral artery.

pected vasoconstrictions but the clinical significance of this was controversial for two reasons: First, temporary vasoconstrictions due to eclampsia could have been stabilized by magnesium sulfate and been difficult to visualize with MR angiography; and second, anatomical variations were frequently observed in the cerebral vasculature. As Rutherford [15] reported, MR angiography may be much less appropriate to assess the functional vascular condition and to monitor cerebral vasospasms than transcranial Doppler ultrasound. According to our data, abnormal MR angiography alone has poor reliability for ascertaining clinical significance.

Emergency cesarian sections were performed on 33 cases, labors were induced in five cases ending in vaginal delivery, and three cases delivered spontaneously. Neonatal prognoses were good for all women after some were transferred to the NICU. All women involved in the study finally recovered without sequelae.

Discussion

Abnormal cerebral images were detected in only 14.3% of severe preeclampsia cases, and so there is little